SMT: SPLIT/MERGE FIBER TRACTOGRAPHY FOR MR-DTI

by

Uğur Bozkaya

B.S. in Civil Engineering, Boğaziçi University, 2002

Submitted to the Institute for Graduate Studies in
Science and Engineering in partial fulfillment of
the requirements for the degree of
Master of Science

Graduate Program in Biomedical Engineering Institute

Boğaziçi University

2006

ACKNOWLEDGEMENTS

I would like to thank Assist. Prof. Burak Acar, my thesis supervisor for all the help and support given throughout the project and Dr. R. Bammer from Stanford University for providing MR-DTI data. I would also like thank Celal Eşli, Ender Konukoğlu, Erdem Yörük, Erhan Durusüt, Barış Özgül, Enver Yağcı for sharing the desperateness and joy of BUSIM.

This thesis is in part supported by grants from Tübitak KARİYER-DRESS(104E035) project and EU 6^{th} Framework SIMILAR NoE.

ABSTRACT

SMT: SPLIT/MERGE FIBER TRACTOGRAPHY FOR MR-DTI

Magnetic Resonance Diffusion Tensor Imaging is a recent imaging modality which has shown promise as a non-invasive tool for estimating the orientation and quantity of white matter tracts in vivo. It has been shown that the estimated diffusion tensor's principal diffusion direction coincides with the fiber orientations, given that the tensor in question is anisotropic. MR-DTI fiber tractography aims at following these principal diffusion directions to reconstruct fiber paths. The conventional approach is to use integration techniques, i.e. to follow the principal diffusion directions.

The goal of this project is to introduce a new technique for estimation and visualization of fiber tracts. The proposed Split/Merge Tractography (SMT) tries to overcome the disadvantages of existing techniques. SMT's approach is to generate short (thus more reliable) fiber tracts by conventional techniques (Splitting step) and then group these short tracks according to an estimated distribution (Merging step). SMT allows branching and does not mask the inherent resolution limitation of the data. The aforementioned distribution is estimated via the Metropolis-Hastings Method.

ÖZET

BÖL/BİRLEŞTİR YÖNTEMİ İLE SİNİR AĞLARININ BULUNMASI

Manyetik rezonans difüzyon tensör görüntüleme yeni gelişen ve müdahale gerektirmeden beyindeki beyaz maddenin yapısını göstermek için kullanılan bir tekniktir. Tensor'ün anizotropik olduğu durumlarda tensorden hesaplanan ana difüzyon yönü ile sinir ağlarının yönünün birbirleriyle çakıştığı gösterilmiştir. Manyetik rezonans difüzyon tensor görüntülemenin amacı hesaplanan bu ana difüzyon yönlerini takip ederek sinir ağlarının oluşturulmasıdır. Genelde kullanılan yöntem integral alma metodlarıdır.

Bu projenin amacı sinir ağlarının hesaplanması ve görüntülenmesi için yeni bir teknik ortaya koymaktır. Önerilen Böl/Birleştir Sinir Ağları Takip yöntemi mevcut olan yöntemlerin dezavantajlarını aşmayı amaçlamaktadır. Böl/Birleştir Sinir Ağları Takip yönteminin yaklaşımı önce kısa sinir ağı parçalarını bilinen yöntemlerle oluşturmak ve daha sonra bu kısa parçaları hesaplanan dağılıma göre gruplandırmaktır. Bu yöntem dallanmaya ve datanın çözünürlüğünü olduğu gibi kullanmaya izin vermektedir. Altta yatan dağılım Metropolis-Hastings yöntemi ile hesaplanmaktadır.

TABLE OF CONTENTS

LIST OF FIGURES

LIST OF SYMBOLS/ABBREVIATIONS

$\vec{e}$	Eigen Vectors
λ	Eigen Values
Π	Fitness Value
CT	Computed Tomography
D	Diffusion Coefficient
$\underline{D}$	Diffusion Tensor
EPI	Echo-Planar Imaging
FA	Fractional Anisotropy
fMRI	functional Magnetic Resonance Imaging
GUI	Graphical User Interface
ITK	Insight Segmentation and Registration Tool Kit
IVOH	Intra-Voxel Orientational Heterogeneity
K	Distance Scaled Mutual Diffusion Coefficient
MRI	Magnetic Resonance Imaging
NMR	Nuclear Magnetic Resonance
PDD	Principal Diffusion Direction
TOI	Tracts of Interest
USB	Universal Serial Bus
VTK	Visualization Tool Kit

1. INTRODUCTION

1.1. Background

Diffusion Tensor Magnetic Resonance Imaging (DT-MRI), also known as Diffusion Tensor Imaging (DTI), has shown promise as a non-invasive tool for estimating the orientation and quantity of White Matter (WM) tracts in vivo. The process of using DTI data to estimate white matter structures is commonly known as tractography. DTI tractography is a unique imaging modality that is a clinically applicable mean of non-invasively imaging the myelinated axonal structure of the human brain. The DT-MRI technique has raised hopes in the neuro-science community for a better understanding of the fiber tract anatomy of the human brain. Various methods have been proposed to use DT-MRI data to track nerve fibers and derive connectivity between different parts of the brain.

The ability of DTI to quantitatively describe white matter connectivity in the human brain has a variety of clinical applications. The correlation between white matter structural asymmetries and schizophrenia is currently being investigated in group studies. Similar group studies are being conducted to gain an understanding of the progression of white matter tract damage in neuro-degenerative diseases such as Alzheimer's disease. Changes in the diffusion directional dependence, known as diffusion anisotropy, have been illustrated to have promise in detecting and characterizing brain tumors. DTI has been used to characterize reductions in diffusion anisotropy in regions of severe brain trauma that are theorized to result from tissue swelling. It is hoped that DTI will provide insights into the progression of tissue damage in cases of severe injury, and that these insights could provide strategies to limit the spread of tissue damage [3].

The goal of this project is to introduce a new technique for estimation and visualization of fiber tracts. The proposed Split/Merge Tractography (SMT) tries to overcome the disadvantages of existing techniques. SMT's approach is to generate

short fiber tracts by conventional techniques (Splitting step) and then group these short tracks according to an estimated distribution (Merging step). The generated short fibers are more reliable since no large error accumulation is allowed. These short fibers help to visualize the local tensor orientation. Advantage SMT is that it allows branching and does not mask the inherent resolution limitation of the data. The distribution is estimated via the Metropolis-Hastings Method.

1.2. Organization of the Thesis

The rest of the thesis is organized as follows: In Chapter 2, a brief introduction on Magnetic Resonance Diffusion Tensor Imaging and its basics is given. A literature survey is presented about the existing techniques and limitations about DTI fiber tractography is given. In Chapter 3, the new approach Split/Merge Fiber Tractography we proposed in this thesis, is explained. In Chapter 4, the proposed technique is tested and compared with existing techniques. Chapter 6 includes information about the software development environment used in this project. Conclusions drawn from the study and suggestions offered for future research are discussed in Chapter 7. Detailed information about the Log-Euclidean framework and Metropolis-Hastings algorithm used for tensor interpolation and distribution estimation are given in Appendix A and Appendix B, respectively.

2. BACKGROUND

2.1. Magnetic Resonance Diffusion Tensor Imaging (MR-DTI)

Magnetic Resonance Diffusion Tensor Imaging is a recent imaging modality which has shown promise as a non-invasive tool for estimating the orientation and quantity of white matter tracts in vivo. It consists of estimating a diffusion tensor $\underline{D}$ within a voxel and then displaying quantities derived from it. It has been shown that phenomenon of an isotropic diffusion of water in anisotropic tissues can be calculated by a series of nuclear magnetic resonance (NMR) pulsed-gradient, spin-echo measurements in different directions. A tissue's three orthotropic axes can be determined from these measurements and those axes coincide with the eigenvectors of the calculated diffusion tensor where the effective diffusivities correspond to the eigenvalues of the tensor $\underline{\mathbf{D}}$ [5].

2.1.1. Diffusion

Diffusion is a microscopic phenomenon arising from thermal motion in which molecules migrate randomly. Molecular diffusion motion is also referred to as Brownian motion. Einstein's relation develops a time distance relationship for a particle undergoing Brownian motion in free space [2].

$$\mathbf{D} = \frac{1}{6\tau}\mathbf{r}^2 \tag{2.1}$$

where $\mathbf{D}$ is a scalar known as the diffusion coefficient, τ is the period of time during which a particle undergoes Brownian motion, and $\mathbf{r}$ is net displacement. The diffusion coefficient $\mathbf{D}$ relates time to the displacement square, and is therefore not a diffusion velocity [10]. In the case of a restrictively bounded environment, particles undergoing Brownian motion are displaced with greater magnitudes in directions parallel to boundaries, and smaller magnitudes in directions across boundaries. Thus, directionally dependent Brownian motion reflects the underlying structure of a bounded

environment. Diffusion is said to be anisotropic when displacement due to Brownian motion is directionally dependent. In cases of anisotropic diffusion, Einstein's relation must be generalized to allow for directional dependence [1],

$$\underline{\mathbf{D}} = \frac{1}{6\tau} < \hat{\mathbf{r}}\hat{\mathbf{r}}^t > \tag{2.2}$$

where $\underline{\mathbf{D}}$ is a second order tensor, and $\hat{\mathbf{r}}$ is a displacement vector indicating both the magnitude and direction of Brownian motion. The tensor $\underline{\mathbf{D}}$ in the generalized form of Einstein's relation is known as the diffusion tensor. The notation <> represents an average over many repeated and uncorrelated measurements. So, Brownian motion is not characterized by the average displacement over sometime, instead by the average displacement squared. In general, the diffusion tensor $\underline{\mathbf{D}}$ depends on particle mass, the structure of the medium and temperature [10]. In DTI, the particle mass of water molecules and the temperature at which measurements are conducted is assumed to be constant. This assumption allows for the spatial fluctuation of the diffusion tensor in DTI to be interpreted solely in terms of local anatomical structure. The process of diffusion may also be viewed at a macroscopic level in terms of a group of moving particles. Fick's first equation describes the effect of diffusion on the motion of nonuniform distributions of particles, as

$$\hat{\mathbf{J}} = -\mathbf{D}\nabla C(\mathbf{r}) \tag{2.3}$$

where $\hat{\mathbf{J}}$ is a vector representing the magnitude and direction of particle flux, $\mathbf{D}$ is the coefficient of diffusion in the $\hat{\mathbf{J}}$ direction, and $C(\mathbf{r})$ is a scalar valued function that describes the concentration of particles at a given position $\mathbf{r}$. Fick's first equation states that the flux of particles in a system is proportional to the gradient of the particle concentration. Therefore, Equation 2.3 predicts an equilibrium of zero particle flux for systems with an even spatial distribution of particles where $C(\mathbf{r})$ is constant. The negative constant of proportionality next to the gradient of $C(\mathbf{r})$ on the right hand side of Equation 2.3 is the basis for the understanding of diffusion as the tendency of particles in a system to move from areas of greater concentration to areas of lesser concentration [2].

2.1.2. Diffusion Tensor

When diffusion is anisotropic, a scalar diffusion measure is insufficient for describing the diffusion properties. It has been shown that the diffusion in this case can be described by a second-order diagonally symmetric tensor, called the diffusion tensor $\underline{\mathbf{D}}$,

$$\underline{\mathbf{D}} = \begin{bmatrix} D_{xx} & D_{xy} & D_{xz} \\ D_{yx} & D_{yy} & D_{yz} \\ D_{zx} & D_{zy} & D_{zz} \end{bmatrix} \tag{2.4}$$

The diffusion tensor defines a principal frame of directions ($\acute{x}$, $\acute{y}$, and $\acute{z}$) for each voxel by its eigenvectors (Figure 2.1). The diffusion displacement profile may be represented as an ellipsoid with the length of principal axes described by the tensor eigenvalues (principal diffusivities λ_1, λ_2 and λ_3) and the directions given by the tensor eigenvectors ($\vec{\mathbf{e}_1}$, $\vec{\mathbf{e}_2}$, and $\vec{\mathbf{e}_3}$). The diffusion eigenvectors are generally not aligned with the laboratory frame. The eigenvector with the highest eigenvalue represents the principal diffusion direction (PDD) at the corresponding position. In the principal component frame, the displacements along $\acute{x}$, $\acute{y}$, and $\acute{z}$ appear uncorrelated and the diagonal elements of the tensor are equal to tensor the eigenvalues [11].

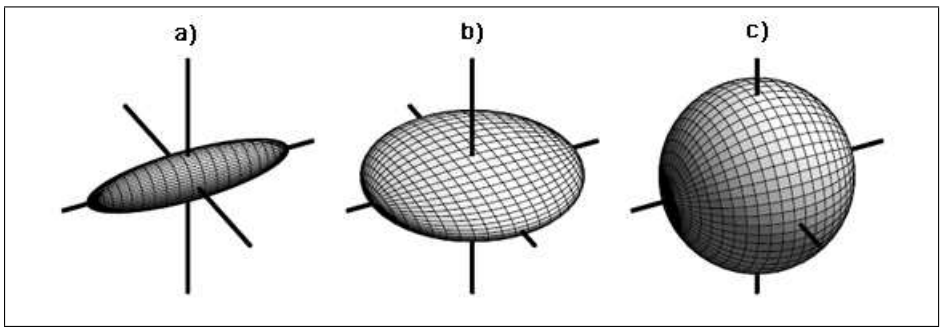

Figure 2.1. Diffusion tensor's eigenvalues are the radii of the ellipsoid, while the eigenvectors determine the orientations of the axes. [3]
a)Linear anisotropic diffusion b)Planar anisotropic diffusion c)Isotropic diffusion

In cases of purely isotropic diffusion, the diffusion ellipsoid takes on a spherical shape, as $\lambda_1 = \lambda_2 = \lambda_3$. There are two extreme cases of physically realizable anisotropic

diffusion in which the ellipsoidal description of Figure 2.1 degenerates. For purely linear anisotropic diffusion, λ_1 = c and $\lambda_2 = \lambda_3 = 0$, the diffusion ellipsoid degenerates into a line pointing in the $\vec{e_1}$ direction. In the case of purely planar anisotropic diffusion, the diffusion ellipsoid becomes plate like shaped, meaning that λ_1, λ_2 ¿ 0, $\lambda_3 = 0$

The degree of anisotropy in the diffusion tensor is commonly represented by Fractional Anisotropy (FA). FA is defined as

$$FA = \frac{\sqrt{3((\lambda_1 - \lambda_2)^2 + (\lambda_2 - \lambda_3)^2 + (\lambda_1 - \lambda_3)^2)}}{\sqrt{2(\lambda_1^2 + \lambda_2^2 + \lambda_3^2)}} \tag{2.5}$$

For physically realizable diffusion tensors with non-negative eigenvalues, the FA of a diffusion tensor is normalized between zero and one. In an extreme case, a FA value of one denotes a diffusion tensor in which λ_1 = c and $\lambda_2 = \lambda_3 = 0$ and diffusion is completely anisotropic in the direction of $\vec{\mathbf{e}}_1$. The fractional anisotropy metric evaluates to zero in the opposite extreme of a completely isotropic diffusion tensor. In general, higher values of FA occur for diffusion tensors in which local diffusion has a higher degree of anisotropy [3].

2.1.3. Calculation of Tensors

The MR signal is usually corrupted by the diffusion of water molecules leading to a small decrease in the measured signal. In diffusion imaging, this effect is magnified by making use of the strongest possible magnetic field gradient applied in one direction *d*. For each slice, at least seven images are collected with different diffusion weightings and gradient directions. Each gradient is typically applied for a duration of several tenths of a millisecond, during which the average water molecule in brain tissue may migrate 10 or more micrometers in a random direction. The irregularity of the motion entails a signal loss due to the magnetic spin phase differences and can be used to quantify the diffusion constant. If S_0 represents the signal intensity in the absence of a diffusion-sensitizing field gradient and S the signal intensity in the presence of a gradient $\mathbf{g} = (g_x, g_y, g_z)^T$, the equation for the loss in signal intensity due to diffusion

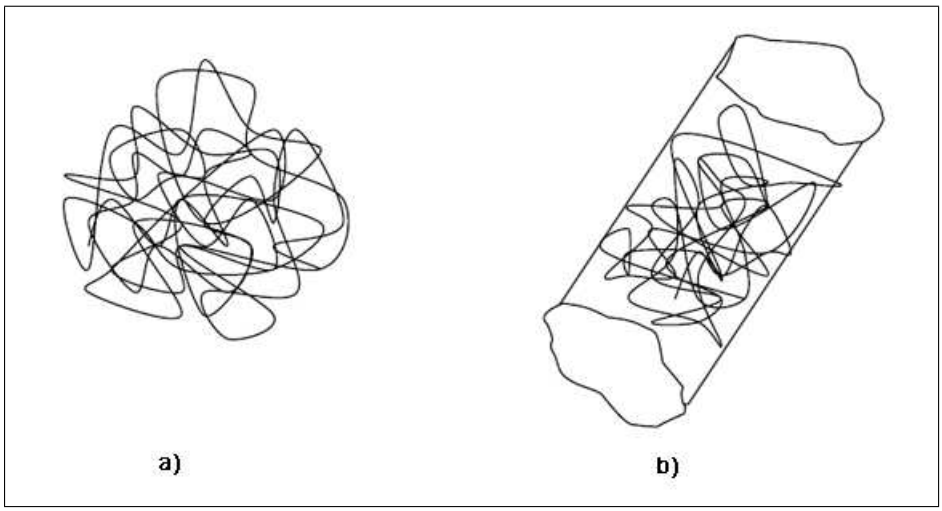

Figure 2.2. Schematic representation of the random walk of a molecule in (a) unrestricted, and in (b) restricted diffusion. The molecular path is perturbed by collisions with other molecules or with medium boundaries such as membranes. [11] . Note the isotropy in the case of unrestricted motion as opposed to the restricted motion.

is given by the Stejskal-Tanner formula

$$ln(S) = ln(S_0) - b\mathbf{g}^T\mathbf{D}\mathbf{g} \tag{2.6}$$

$$b = \gamma^2\delta 2(\Delta - \delta/3) \tag{2.7}$$

where γ is the gyromagnetic ratio of hydrogen ^1H, δ is the duration of the diffusion sensitizing gradient pulses and Δ is the time between the centers of the two gradient pulses. The seven images provide seven equations for S in each voxel, i.e. the smallest sampled part of a 3-D image. The equations are solved in a least-squared sense for the 6+1 unknowns, which corresponds to the six independent components of the symmetric diffusion tensor, $\underline{\mathbf{D}}$, and S_0 [9].

2.2. Fiber Tractography in MR-DTI

Neurons are the physical structures in the nervous system that transmit information in the form of nerve impulses from one part of the body to another. Neurons are composed of three basic parts: the cell body, the axon, and the dendrites. The dendrites are attached to the neuron cell body, and receive impulses from other neurons at synapses. Axons are long cable-like structures that transmit impulses away from the dendrites and the cell body. Axons are wrapped by a thin layer of connective tissue known as the endoneurium. Groups of wrapped axons are bundled together into tracts, or fascicles, by a thin boundary known as the perineurium [3].

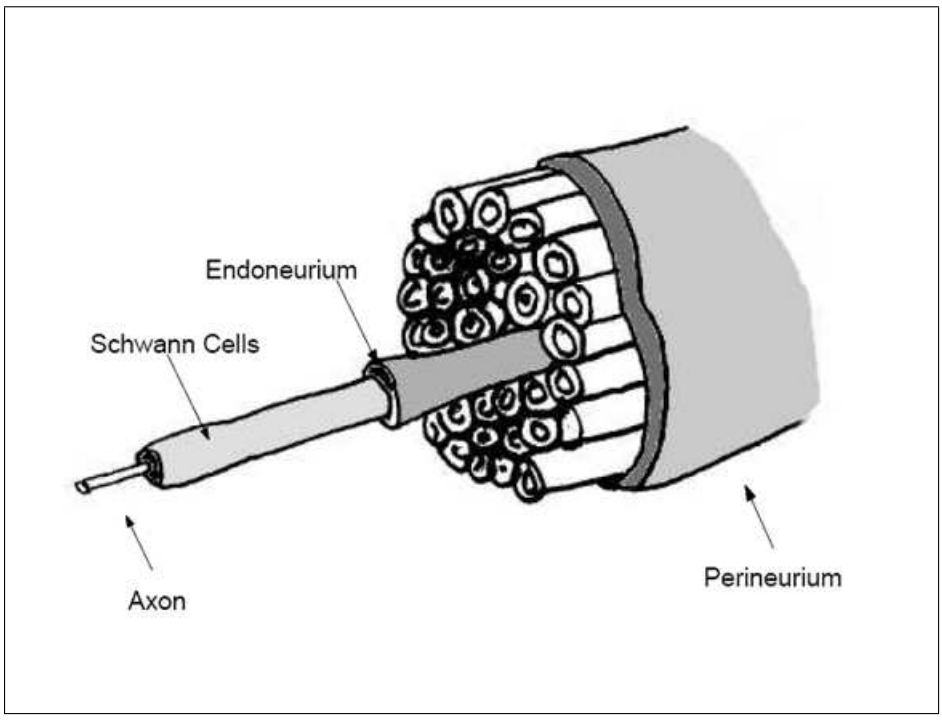

Figure 2.3. Illustration of myelinated fiber tract [3]

The portion of the fascicles in the human brain that contain white fatty myelinated Schwann cells form the white matter of the brain. The mobility of water to diffuse across tracts with myelinated boundaries is restricted, causing water to diffuse anisotropically in greater amounts in directions parallel to fiber tracts and lesser amounts of diffusion in directions across the boundaries. This physical situation of increased water diffusion in directions parallel to myelinated fascicles is what is measured by diffusion weighted imaging to construct diffusion tensors [3]. The principal eigen-

vector of the estimated diffusion tensor, i.e. the principal diffusion direction coincides with the fiber orientation. Fiber tractography refers to constructing the fiber paths based on the information in diffusion tensors. Figure 2.4 shows a tensor field and the corresponding diffusion tensors.

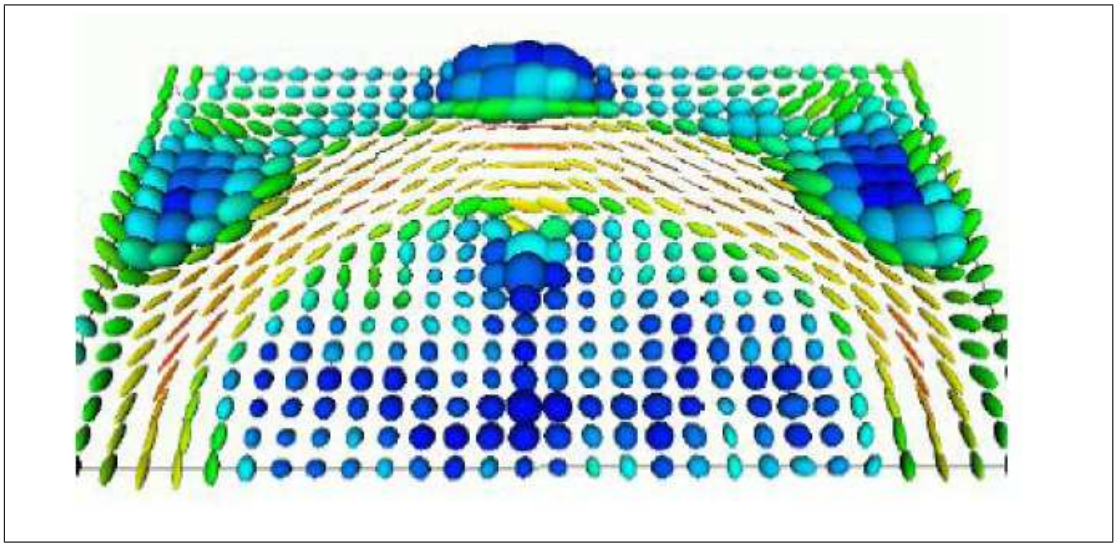

Figure 2.4. Visualization of tensor field [34].

2.3. Current Fiber Tractography Approaches

2.3.1. Numerical Integration

It is proposed that a white matter fiber tract trajectory could be represented as a 3D space curve, i.e., a vector parameterized by the arc length, $\mathbf{s}$, of the trajectory [7].

$$\frac{dr(\mathbf{s})}{d\mathbf{s}} = t(\mathbf{s}) \tag{2.8}$$

where $t(\mathbf{s})$ is the unit tangent vector to $r(\mathbf{s})$ at $\mathbf{s}$. These vectors are depicted in Figure 2.5. They also claimed that the normalized eigenvector, ε_1, associated with the largest eigenvalue of the diffusion tensor, $\underline{\mathbf{D}}$, λ_1, lies parallel to the local fiber tract direction in coherently organized white matter. The key idea in this tracking algorithm is to equate the tangent vector, $t(\mathbf{s})$, and the unit eigenvector, ε_1, calculated at position

$r(\mathbf{s})$:

$$t(\mathbf{s}) = \varepsilon_1(r(\mathbf{s})) \tag{2.9}$$

Combining the Equations 2.8 and 2.9, we obtain:

$$\frac{dr(\mathbf{s})}{d\mathbf{s}} = \varepsilon_1(r(\mathbf{s})) \tag{2.10}$$

This system of three implicit (vector) differential equations is solved for the fiber tract trajectory subject to an initial condition:

$$r(0) = r_0 \tag{2.11}$$

which specifies a starting point on the fiber tract. We can use different numerical methods to solve for $r(\mathbf{s})$, such as Euler's Method and the Runge-Kutta Method.

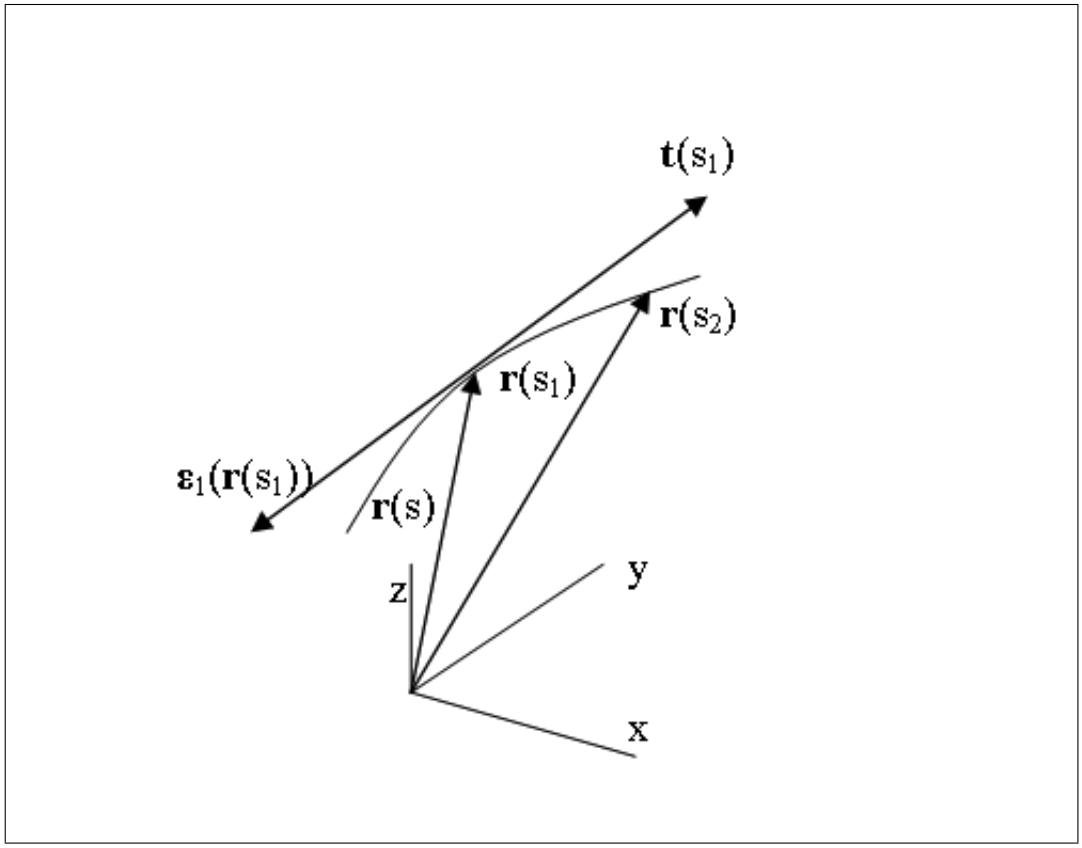

Figure 2.5. Representation of a white matter fiber tract as a 3D space curve [7]

2.3.1.1. Euler's Method. In Euler's Method, a point is chosen on $r(\mathbf{s})$, $r(\mathbf{s}_0)$ and the diffusion tensor there $\underline{\mathbf{D}}(r(\mathbf{s}_0))$ is calculated. Then the next point on the fiber tract is approximated by using a Taylor series expansion of $r(\mathbf{s})$ about $r(\mathbf{s}_0) : r(\mathbf{s}_1) = r(\mathbf{s}_0) + r'(\mathbf{s}_0)(\mathbf{s}_1 - \mathbf{s}_0) + ...$. Since the slope of $r(\mathbf{s}_0)$ at $\mathbf{s}_0$, $r'(\mathbf{s}_0)$, is assumed o be parallel to $\varepsilon_1(r(\mathbf{s}_0))$, for some small number α (with $0 < |\alpha| < 1$), $r'(\mathbf{s}_0)(\mathbf{s}_1 - \mathbf{s}_0) \approx \alpha\varepsilon_1(r(\mathbf{s}_0))$. Once α is chosen, the following equation can be written:

$$r(\mathbf{s}_1) \approx r(\mathbf{s}_0) + \alpha\varepsilon_1(r(\mathbf{s}_0)) \tag{2.12}$$

Thus $r(\mathbf{s}_1)$ can be estimated from values of $r(\mathbf{s}_0)$ and $\varepsilon_1(r(\mathbf{s}_0))$. This routine can be repeated to find all the points along the path of a singe fiber tract $r(\mathbf{s})$ [12].

2.3.1.2. Runge-Kutta Method. Euler's method is easy to explain and to implement but on the other hand it is accurate only to the 1^{st} order, and susceptible to large error accumulation and numerical instabilities. Since the diffusion tensor $\underline{\mathbf{D}}(x)$ can include 2^{nd} and higher derivatives of $\varepsilon_1(x)$, it is better to use this information in a more robust and accurate numerical method to integrate the fiber tract paths. Using Runge-Kutta integration, a similar equation to Euler's can be employed to calculate $r(\mathbf{s}_0)$, the next point on the fiber tract path [12] [7].

$$\mathbf{r}_{n+1} \approx \mathbf{r}_n + hV_{n+1} \tag{2.13}$$

where

$$V_{n+1} = \frac{1}{6}(k_1 + 2k_2 + 2k_3 + k_4) \tag{2.14}$$

$$k_1 = \frac{V_n \cdot \varepsilon_1(r_n)}{|V_n \cdot \varepsilon_1(r_n)|}\varepsilon_1(r_n) \tag{2.15}$$

$$k_2 = \frac{V_n \cdot \varepsilon_1(r_n + h/2k_1)}{|V_n \cdot \varepsilon_1(r_n + h/2k_1)|}\varepsilon_1(r_n + h/2k_1) \tag{2.16}$$

$$k_3 = \frac{V_n \cdot \varepsilon_1(r_n + h/2k_2)}{|V_n \cdot \varepsilon_1(r_n + h/2k_2)|}\varepsilon_1(r_n + h/2k_2) \tag{2.17}$$

$$k_4 = \frac{V_n \cdot \varepsilon_1(r_n + hk_3)}{|V_n \cdot \varepsilon_1(r_n + hk_3)|}\varepsilon_1(r_n + hk_3) \tag{2.18}$$

A trajectory is terminated when it reaches the edge of the data defined. Unfortunately,

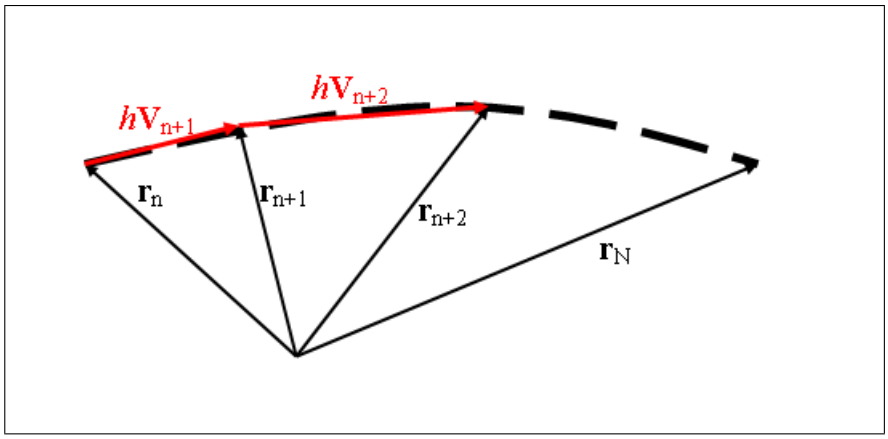

Figure 2.6. The principle of tractography [7]

the reliability of the tracking is compromised by the noise and degree of partial volume effect in the image, meaning that trajectories tend to jump between adjacent structures. This usually happens when a trajectory undergoes a sharp change in direction [12]. A maximum allowable rate of change of direction is generally applied, accepting only gentle curvature along the trajectory, in an attempt to constrain the path to one structure only. Also when a trajectory reaches a region with low diffusion anisotropy value such as FA¡0.15, it is immediately terminated.

2.3.2. Interface Propagation

Parker et al. applied level set theory using fast marching methods to generate a 3D time of arrival maps from which connection paths between brain regions can be

identified. This approach allows branching and determines how reasonable or likely any path is in representing a "true" pathway of connection. Maps showing the time of arrival of a propagating front from a starting point, may be determined for the whole brain. From this information, paths can be extracted [13]. The fast marching method is governed by the Eikonal equation (2.19):

$$|\nabla T|\, F = 1 \tag{2.19}$$

where T is the time of arrival, F is the propagation speed function.

The evaluation of front using fast marching method as seen in Figure 2.7 allows a time of arrival, T, from the seed point to any point in the image volume, to be determined. The rate F, at which the front propagates from the starting point is linked to the PDD field. Each iteration involves the determination of F($\mathbf{r}$) where $\mathbf{r}$ is the position of the voxels on the propagating front during the p^{th} iteration. Two different F definitions are implemented. The first one is regarded as a measure of voxel similarity and is defined as

$$F_1(r) = \frac{1}{1 - min((|\varepsilon_1(r) \cdot n(r)|), (|\varepsilon_1(\acute{r}) \cdot n(r)|), (|\varepsilon_1(r) \cdot \varepsilon_1(\acute{r})|))} \tag{2.20}$$

where $\acute{\mathbf{r}}$ is the position of a voxel neighboring $\mathbf{r}$ that has already been passed by the front. $\acute{\mathbf{r}}$ is chosen to be the neighbor for which ($\mathbf{r}$-$\acute{\mathbf{r}}$) is most closely aligned with the direction of the normal to the front $n(\mathbf{r})$. This assures that front propagation will occur fastest if both $\varepsilon_1(r)$ and $\varepsilon_1(\acute{r})$ are close to collinear with $n(r)$ and close to collinear each other, therefore pointing toward each other. Front evolution will be fastest along the white matter tracts where strong coherence between $\varepsilon_1(\mathbf{r})$ in the neighboring voxels is observed. The other version of F is based on the idea of embedded connectivity information.

$$F_2(r) = min(F_2(\acute{r}), (|\varepsilon_1(\acute{r}) \cdot n(r)|)) \tag{2.21}$$

In this definition, $F_2(\acute{\mathbf{r}})$ term provides a memory of previous iterations of the front

position. This can be interpreted as embedding connectivity information already established between the seed point and $\acute{\mathbf{r}}$ in the value of F_2. After calculating the T map

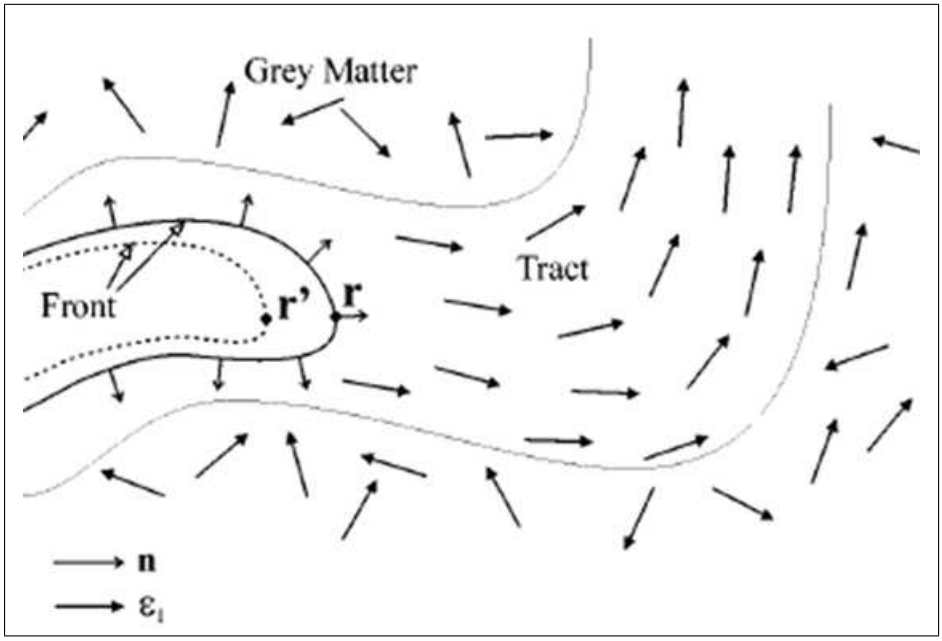

Figure 2.7. Vectors used in the calculation of the speed function [13]

for a seed point, fiber paths are obtained by backtracking which is shown in figure 2.8. Since each point in T may be connected to the seed point, a true anatomical connectivity may be estimated by determining a connectivity metric and regarding only those paths whose metric is above a specified threshold, as a true anatomical connectivity [13]. In this approach, the problem of having regions with low anisotropy values due to the presence of crossing fibers can be solved. While the fast marching method is able to continue through such regions and find the true pathways of interest, the possibility of false positives can not be ignored. This approach can be improved through new definitions of speed function F since the implementations currently rely on ε_1 values only.

Another approach, geometric flows, is introduced by Campbell for the segmentation of fibertracts [14]. These flows are designed to evolve closed surfaces in 3D so as to increase the flux of a fixed vector field (the PDD field) through them at the fastest possible rate with respect to a Euclidean length or area metric. A two dimensional representation is shown in Figure 2.9. The total inward flux of the vector field through

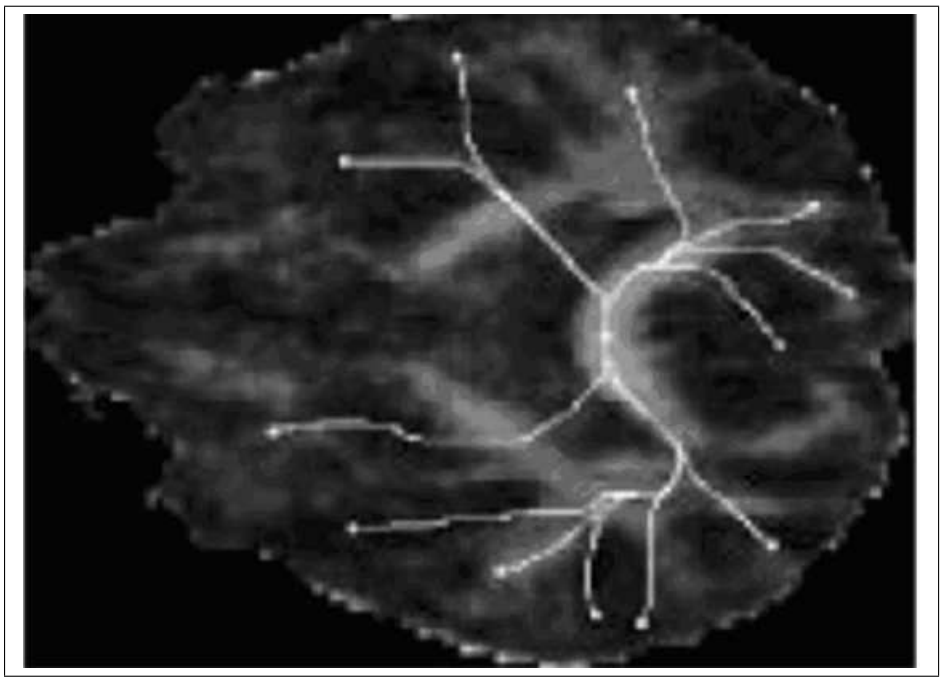

Figure 2.8. Paths from arbitrary point to seed point using gradient descent through T map [13]

the curve is given by contour integral

$$Flux(t) = \int_0^1 \langle V, N \rangle \, \|C_p\| \, d_p = \int_0^{L(t)} \langle V, N \rangle \, ds \tag{2.22}$$

where N is the unit inward normal of closed curve C parametrized by p and s is the arc length parametrization of the curve in the vector field $V = (V_1(x, y, z), V_2(x, y, z))$, and L(t) is the Euclidean length of the curve. Parker et al. proposed that the gradient flow that maximizes the rate of increase of the total inward flux with respect to the Euclidean arc length is obtained by moving each point of the curve in the direction of the inward normal by an amount proportional to the divergence of the vector field. Rather than explicitly calculating the divergence of the extended vector field, the numerical computation can be made much more robust by resorting it to an integral form. Let ΔV be a volume, dV a volume element, dR its bounding surface, N the outward normal at each point on the surface and dS a surface area element [14]. Via the divergence

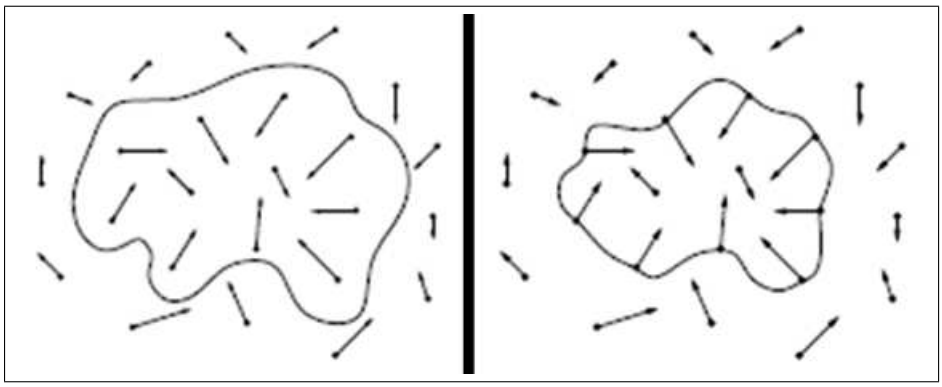

Figure 2.9. Left: A closed planar curve is placed in a 2D vector field. Right: The curve evolves so as to increase the inward flux through its boundary as fast as possible [14].

theorem,

$$\int_{\Delta V} div(V)dV = \int_{dR} \langle V, N \rangle \, dS \tag{2.23}$$

In other words, the integral of the divergence of a vector field over a volume is given by its outward flux through that region's bounding surface. The key benefit of this method is that it has the ability to reconstruct multiple fibers in parallel, instead of taking an iterative approach where the complexity of the algorithms increases as the number of tracts to be reconstructed increases. It deals well with arbitrary numbers of branches and merge points. It may be preferable to use all of the information in the diffusion tensor instead of only the principle eigenvector [14].

2.3.3. Diffusion Simulation

Hagmann used the idea that the brownian movement of water molecules in the brain can be described by a random walk model. It means that the particle trajectory is made of a succession of jumps that are the realization of a random variable. In an infinite homogeneous medium the distribution of the random variable is an isotropic three dimensional Gaussian function whose variance is proportional to the diffusion coefficient (Einstein, 1956). But the living tissue is highly structured and highly compartmented for water particles. Under those circumstances, the diffusion function

deviates from an isotropic Gaussian and becomes a complicated function of position and diffusion time [15]. The developed statistical fiber tracking algorithm is based on two hypotheses:

- Considering a voxel, the probability of a fiber to propagate in a given direction is proportional to the corresponding diffusion coefficient.
- Trajectories of axonal bundles follow regular curves.

Based on these two hypothesis, a random walk model and diffusion tensor field $\mathbf{D}^{\alpha}$ of a particle diffusing in a non homogeneous medium is constructed with a curve regularizing constraint emphasizing collinearity with $\mathbf{r}_i$, a random vector uniformly distributed over a unit sphere.

$$q_{i+1} = q_i + h\Omega_i \tag{2.24}$$

$$\Omega_i = \frac{hd_i + \Omega_{i-1}}{\|hd_i + \Omega_{i-1}\|} \tag{2.25}$$

$$d_i = \underline{D}_i^{\alpha}\mathbf{r}_i \tag{2.26}$$

The curve that the particle propagation generates grows along a unit vector Ω_i, that is a random direction vector modeling the statistical nature of the diffusion process and the curve regularizing constraint. Equation 2.24 explains this procedure where q_{i+1} is the next point and q_i is the current point on the path. The next point on the path is in the Ω_i direction with a step size defined by h. This is the standard numerical integration method to follow the underlying vectors. The methods differ in the calculation of step direction, namely Ω_i, here.

The random vector $\mathbf{d}_i$ is defined on the unit sphere and distributed according to the local diffusive properties which is obtained from Equation 2.26. α is an anisotropy enhancing exponent. It is a power to the diffusion matrix $\underline{\mathbf{D}}$ [15]. If α is put to 1

the algorithm gives a lot of weight to possible fiber trajectories deviating from the main direction and provides random jumps by increasing the weight of $\mathbf{r}_i$, which is uniformly distributed over a unit sphere. Whereas, if α is large, the distribution is tightened around the main eigenvector in which case the propagation rule comes close to a classic PDD fiber tracking.

The step direction Ω_i is a weighted sum of the random vector d_i, and the previous displacement vector Ω_{i-1}, which enhances collinearity.

This approach has the following advantages to the classical ones; the nature of the data is better taken into account, the sensitivity to noise is decreased and the possibility of fiber crossing and diverging is introduced. However, an uncertainty concerning the trajectory of individual fibers appears. Each curve should not be interpreted as a precise mapping of a real axonal trajectory. Selected fibers should be considered together and areas of high fiber density as very likely trajectories whereas projections of few fibers may not correspond to an anatomical entity. In that sense, the statistical density mapping seems a complementary tool to the trajectory maps in the context of statistical fiber tracking, in order to evaluate the validity of the fibers passing through a given region [15].

Another simulation approach, proposed by Yörük, is based on energy minimization task. Yörük associates the diffusion tensor field to a physical system composed of nodes and springs, with their constants defined as a function of local structure [16]. A model based on a physical setup of massless nodes (voxels) and springs is proposed where springs, which link adjacent nodes (voxels) of the domain, act as local "connection" units as shown in Figure 2.10. Their stiffness varies in correlation with DT-MRI data, i.e. with the amount of "connectedness" of the underlying tensors, which is measured in terms of the so called "mutual diffusion coefficient", a novel metric that approximates the ellipsoidal volume overlap of a given tensor pair. A second set of springs with a spatially constant stiffness, is introduced to oppose the effect of the previous ones by linking each node to a virtual ground and acting as "inertia" units. It is showed that the connectivity map associated to this physical system can be achieved

by minimizing its total potential energy, with the seed node being lifted to a temporally constant height and others initially kept at the ground, where node height is defined as an indicator of connectivity [16]. Connectivity of two given tensors located at $\mathbf{r}_1$ and $\mathbf{r}_2$ is defined as

$$K_{12} = \frac{\left[(v^T \underline{D}_1 v)(v^T \underline{D}_2 v)\right]^\gamma}{\delta^2} \tag{2.27}$$

Where $v = (\mathbf{r}_1 - \mathbf{r}_2)/\delta$ and $\delta = \|\mathbf{r}_1 - \mathbf{r}_2\|_2$. Thus, K reflects the mutual influence of tensor pairs by giving the distance scaled product of their diffusion coefficients evaluated in the unit direction of their Euclidean link and raised to the power γ which is used as an enhancement parameter. With this model, total potential energy stored

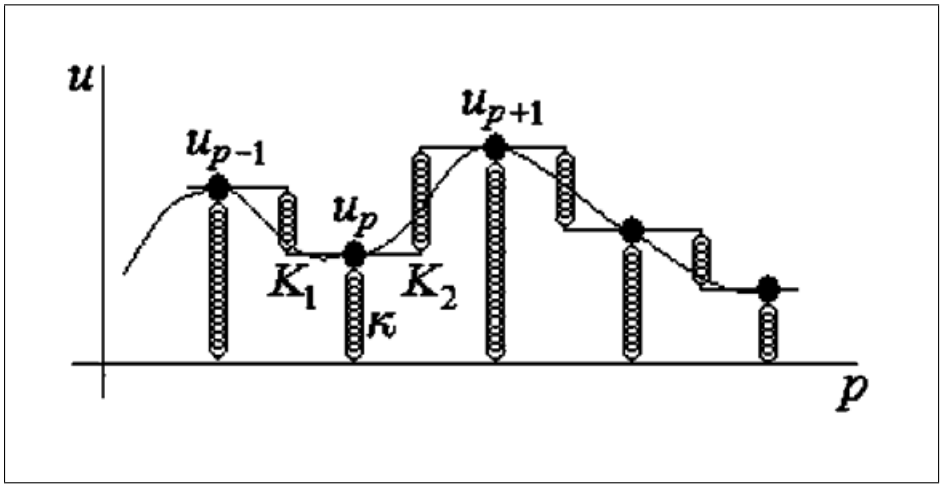

Figure 2.10. Illustration of proposed spring system for a 1D curve (solid line), dots represent the nodes, spring constants are given for the specific node u_p. [16]

at 7 springs considering the 6 voxel neighborhood is given as:

$$V_{springs} = \frac{1}{2}\kappa u^2 + \sum_{n=1}^{6} V_n \tag{2.28}$$

$$V_1 = \frac{1}{2} K_1 \left[u(x,y,z) - u(x-\delta,y,z)\right]^2 \tag{2.29}$$

and where V_2, V_3, V_4, V_5, V_6 are defined similarly.

$$V(u, u_x, u_y, u_z) = \frac{1}{2}(\kappa u^2 + d_{11}^2 u_x^2 + d_{22}^2 u_y^2 + d_{33}^2 u_z^2) \tag{2.30}$$

Equation 2.30 is obtained by inserting K_n's common denominator δ^2 into the squared elongation terms and taking the limit. d_{jj} are the diagonal elements of diffusion tensor $\underline{D}$. When the current problem can be put into a variational one [16], the connectivity map u with respect to the seed at (x_0, y_0, z_0) can be found by minimizing the following discretized energy functional:

$$J(u) = \sum_p \left\{ \kappa u_p^2 + \frac{1}{2} \sum_{n=1}^{N} K_{pn}(u_p - u_{pn})^2 \right\} \tag{2.31}$$

where p is the voxel index and N is the number of neighbors. u_{pn} and K_{pn} stand for the n^{th} neighbor of the p^{th} node and its associated spring constant, respectively. One advantage of this method is that it is computationally inexpensive. Also it provides a tuning parameter, γ to weight the usage of principal direction versus the whole diffusion tensor data usage. The converged results of the calculated connectivity maps with different γ values are shown in Figure 2.11.

2.4. Limitations of Conventional Fiber Tractography

Current hardware limitations in MRI scanners limit the spatial resolution in DTI data to the order of one millimeter. So, DTI tractography is a macroscopic model of a microscopic structure. Therefore, DTI tractography estimates are macroscopically sampled descriptions of underlying microscopic structures. The under-sampling of the underlying white matter structure in DTI data gives rise to Intra-Voxel Orientational Heterogeneity (IVOH) [1], a condition in which white matter structures of multiple different orientations are averaged into a single DTI voxel sample, causing a loss of validity in the diffusion tensor model. This is called partial volume effect. The effect is important, especially, where fiber crossing, kissing or branching is seen in a voxel. In many cases, partial volume effects become less apparent with increased spatial res-

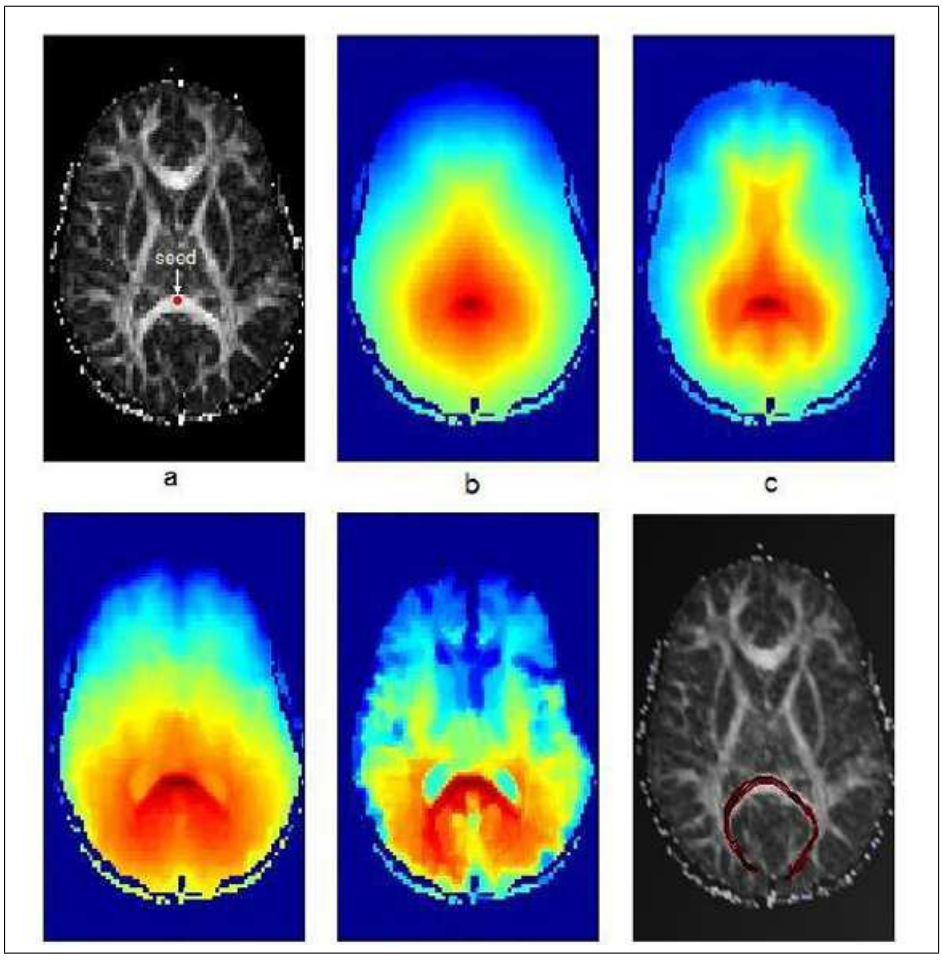

Figure 2.11. a) Axial slice of FA map with the seed indicated, b) Converged connectivity map (γ= 1), c-e) Converged maps for γ= 2, 4, 10, f) computed tracts for γ= 10. [16]

olution. Limited angular resolution and partial volume effects make it difficult for fiber tracking algorithms to extract the correct fiber orientations in some voxels and thereby making it difficult to track fiber paths in a correct way. While there are strong indications that DT-MRI reveals information of the fiber pathways in the brain, it is important to stress the fact that the explicit quantity measured is water diffusion and not the fibers.

An alternative approach to increase the spatial resolution is to increase the number of directions in which the diffusion is measured and then fit this data to a different, higher order model than the second order tensor. This high angular resolution diffusion imaging holds the promise to be able to determine the directions of multiple

fibers within a single voxel, but also leads to increased acquisition times. Currently, the most common acquisition scheme for acquiring diffusion tensor data is that of echo-planar imaging (EPI) [4]. While this technique is fast, acquiring an entire image in approximately 200ms, it is also susceptible to degradation due to non-uniformities in the magnetic field strength. Since the magnetic field is altered by the presence of structures within the human subject, they cannot be eliminated. However, work is underway to reduce the imaging artifacts using different data acquisition schemes and post processing of the data.

Artifacts can be also introduced while smoothing noisy DTI data. Generating a continuous approximation to the tensor field can introduce phantom connections between tracts which do not exist anatomically. Unconsidered noise in the DWI scan also has adverse effects on tractography. It can cause one to sort eigenvectors incorrectly. This can result in a sudden 90 degree deviation in the computed trajectory which can cause the trajectory to jump to other tracts.

Another drawback of this low resolution image volume is faced during the interpolation process to obtain an increased resolution of the DTI data. Since DTI data is not a scalar value and it is represented as a second order symmetric tensor, an interpolation problem arises. The simplest method is componentwise trilinear interpolation. In this scheme the value of a tensor at any point inside the voxel is a linear combination of the values at its corners and is completely determined by them. Since the coefficients of this linear combination are independent of the tensor indexes, the linear combination of the tensors can be done component-wise. However, more sophisticated interpolation methods would better preserve the eigenvalues along an interpolation path. Component-wise interpolation of eigenvectors and eigenvalues themselves would not lead to correct results, since a linear interpolation between two unit vectors is not a unit vector anymore - the interpolated eigenvector value would leave the manifold of unit vectors. In addition, there can be a correspondence problem in the order of the eigenvalues.

3. SPLIT/MERGE FIBER TRACTOGRAPHY

3.1. Aproach

The new Split/Merge fiber tractography (SMT) approach presented in this thesis overcomes some disadvantages of conventional tractography explained in Chapter 2.3. This new approach relies on the calculated short fiber tracts (strings) which are highly reliable. These short fiber tracts are calculated for seed points with high fractional anisotropy values. Figure 3.2 shows the calculated strings in the whole brain.

3.2. Method

In the calculation of fiber strings, 4^{th} order Runge-Kutta integration is used. Starting from a seed point only very short paths are tracked even if the terminated point of the string has high FA value or the tract continues in a smooth path both in backward and forward directions. This is illustrated in Figure 3.1. Keeping the tracts short prevents the accumulation of error in each string. In the implementation, we choose all the voxels with FA larger than 0.50 as seeds for short tracts, and terminate tracking if the angle between two consecutive steps exceed 20 degrees or FA values drops to 0.25 or maximum step count of 3 is reached. The backward and forward tracks for a seed point are combined to obtain the resulting strings of 6 steps long. A step size of 0.89 mm which is smaller than half of the voxel's smallest dimension is used. To ensure that tracking remains within the brain and skull, a threshold is applied to the anatomical base image. The voxels that are part of a composed string, are excluded from the potential seed set.

The string computation, as described above, requires interpolation of the tensor data. Since DTI data is not a scalar value and it is represented as a 2^{nd} order symmetric tensor, the interpolation is not trivial. The simplest method is component wise trilinear interpolation. However component-wise interpolation of eigenvectors and eigenvalues themselves would not lead to correct results, since a linear interpolation

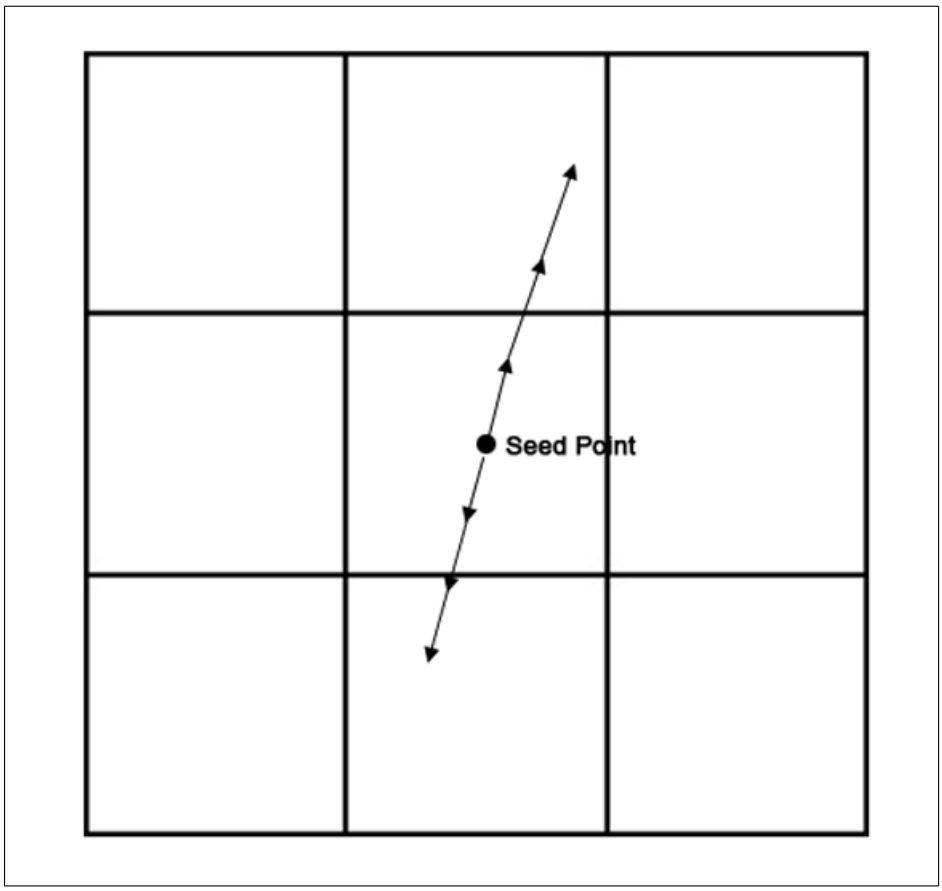

Figure 3.1. Tracking of short fiber strings starting from center of the seed voxel.

between two unit vectors is not a unit vector anymore - the interpolated eigenvector value would leave the manifold of unit vectors. In addition, there can be a correspondence problem in the order of the eigenvalues. In the string computation, we used Log-Euclidean framework for the interpolation of the tensors on the paths [22]. The Log-Euclidean framework prevents the loss of anisotropy during interpolation of tensors. More information about Log-Euclidean framework can be found in Appendix A. Other techniques such as interpolating principle eigenvectors causes loss of information through out the track.

The key idea of SMT is the creation of the co-occurrence matrix $\mathbf{M}$. This matrix is a symmetric NxN sparse matrix where N is the number of calculated strings in the whole volume. $\mathbf{M}_{jk}$ refers to the probability that j^{th} and k^{th} strings are grouped together (i.e. are on the same fiber bundle). Since the matrix is symmetric $\mathbf{M}_{jk}$=$\mathbf{M}_{kj}$.

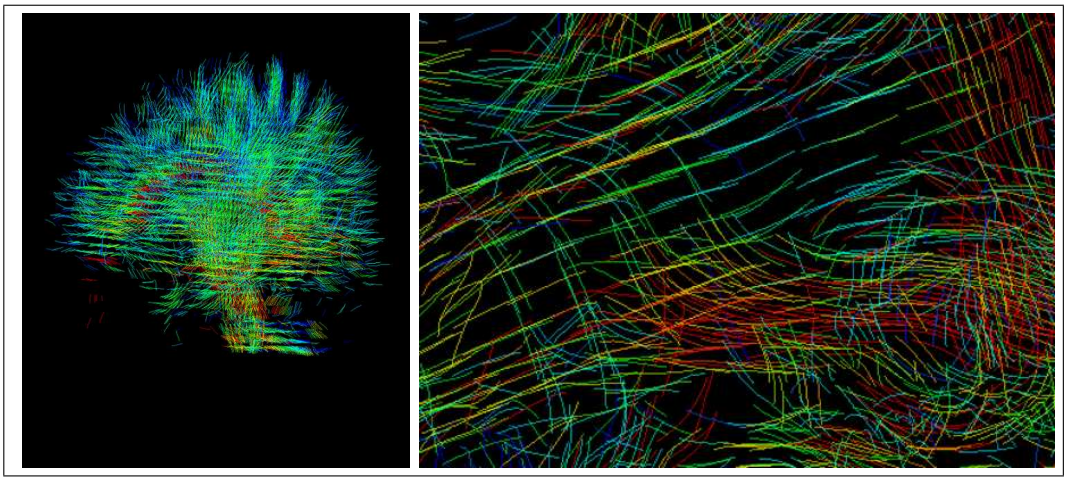

Figure 3.2. Left: Whole fiber strings. Right: Calculated fiber strings in detail

Another way to interpret M_{jk} is

$$\mathbf{M}_{jk} \approx b \times Prob(S_j|S_k) \tag{3.1}$$

where b is a constant scaling factor, and S_j, S_k refer to the j^{th} and k^{th} strings, respectively.

During the visualization, user choses one or more strings of interest,the seed strings. The SMT software selects only the strings that has a non zero value in the co-occurrence matrix for the selected seed strings and displays them. Also, the user can apply a threshold to the co-occurrence matrix and visualize only the strings that are highly probable of being in the same group as shown in Figure 3.3.

Two methods are used in the construction of the co-occurrence matrix: Direct Computation and Metropolis-Hastings Approach.

3.2.1. Method 1: Direct Computation

In the direct computation of the co-occurrence Matrix, a seed string is selected and then the path is grouped starting from this seed string. In each step, the next string is selected according to the probability of diffusing from the end point of current

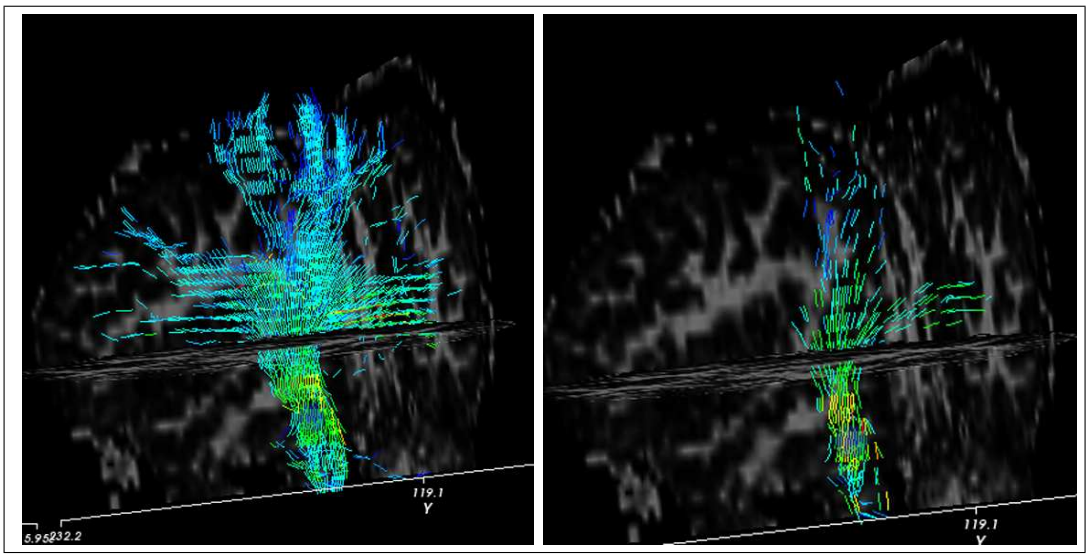

Figure 3.3. Left: String groups are visualized seeding from the stem of Pyramidal Tracks. Right:A threshold value is applied to visualize more probable string groups.

string to the head of the next string. A set of strings are tested in a spherical region at the end point of the current string, within a radius of 3 voxels. The probability of moving from the current point to the target string is calculated with Equation 3.2 which is the fundamental solution of the diffusion Equation 2.3.

$$c(\mathbf{r}) = \left(\frac{1}{4\pi D}\right)^{3/2} exp\left[\frac{-|\mathbf{r}|^2}{4\pi D}\right] \tag{3.2}$$

$$D = v^t \underline{D} v \tag{3.3}$$

where v is the vector in the direction of moving from current location to the candidate string location. The most probable string head is accepted as the next string on the path and the same procedure is repeated. When the probability of jumping to a new string is below a threshold or there are no candidate strings in the search region, the merging is terminated. The merging is performed both in forward and backward directions from the seed string. After merging, for each combination of string pairs the corresponding elements of the co-occurrence matrix are increased by one. The same process is repeated for each string in the volume, considering it as the seed string.

The pseudo code for the Direct Computation Method is as follows:

1. Select a seed string, label it as current string and add its index to the group list
2. Set the direction forward
3. Take a spherical volume in the current direction of current string
4. For each candidate string in the selected volume calculate the probability of moving from current string location to the candidate location
5. If there is no string to be accepted
    - Terminate progress in the current direction and go to step 8
6. Else
    - Accept the string with highest probability and add its index to the group list
    - Make the accepted string the current string and goto 3
7. End if
8. If the current direction is forward
    - Set the current direction as backwards, set the seed string as current string, and go to step 3
9. Else
    - Terminate grouping
10. End if

3.2.2. Method 2: Metropolis-Hastings

The Metropolis-Hastings algorithm is used to generate a sequence of samples from an unknown probability distribution of one or more variables. The purpose of such a sequence is to approximate the distribution (as with a histogram), or to compute an integral (such as an expected value). This algorithm is an example of a Markov Chain Monte Carlo algorithm [23].

The Metropolis-Hastings algorithm can draw samples from an unknown distribution $p(x)$, requiring only that a candidate generating density is known. This means that we only need to know how to generate a new sample from a given sample. The

algorithm generates a set of states x^t which is a Markov chain because each state x^t depends only on the previous state x^{t-1}. The algorithm depends on the creation of a proposal density $q(x^{'}; x^t)$, which depends on the current state x^t and which can generate a new proposed sample $x^{'}$ [23]. Details about the Metropolis-Hastings algorithm can be found in Appendix B.

In SMT, instead of moving to the most probable string from the seed string (as in done in Direct Computation Method) we applied Metropolis-Hastings algorithm to allow random jumps with different probabilities. Comparing to the Direct Computation method, this approach allowed us not to tract only the expected path of the probability distribution of paths that is seeding from a selected string , but it also considers the paths which have lower probabilities of passing through the seed string.

In the implementation of this approach, we start from a seed string and find a group of strings using the direct computation method as shown in Figure 3.4. This group of strings refers to the group that is composed of strings (s_k) and jumps ($b_{k,k+1}$) connecting those strings.

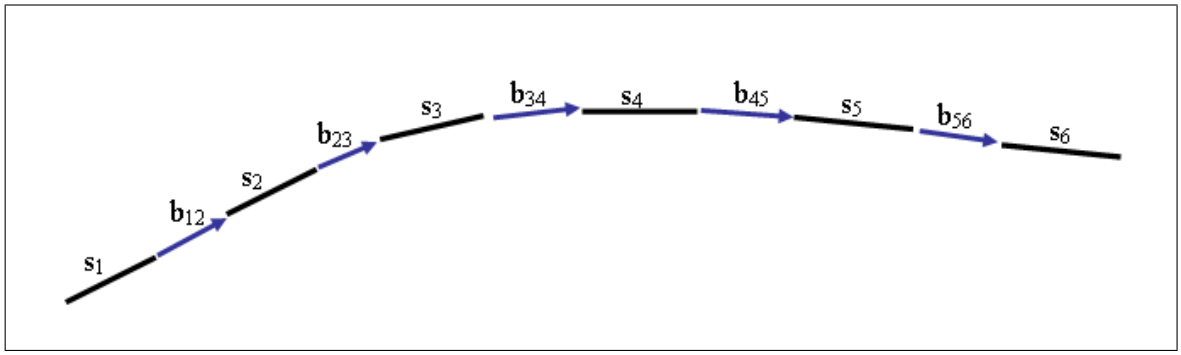

Figure 3.4. The group of strings where s denotes strings and b denotes the bridges connecting those strings

Each jump has a fitness value F_k, equal to the FA value at the starting point of the jump. Thus, jumps that are made over low FA regions are less reliable. A group fitness is set as the minimum jump fitness in that group and is denoted by $f(\underline{x})$.

Metropolis-Hastings algorithm requires sample generation for a given pdf. In SMT, a single group of strings and jumps is a sample. Generating a new sample is achieved by selecting a jump to break the formed group and reestablishing a new jump at that location. The jump to break the group is selected at a random location with a probability inversely proportional to the fitness value at that location. That is, if a jump is made from a low FA location then it is more likely that the group is going to be cut from this location. The half of the group that has the seed string, as shown in Figure 3.5, is preserved.

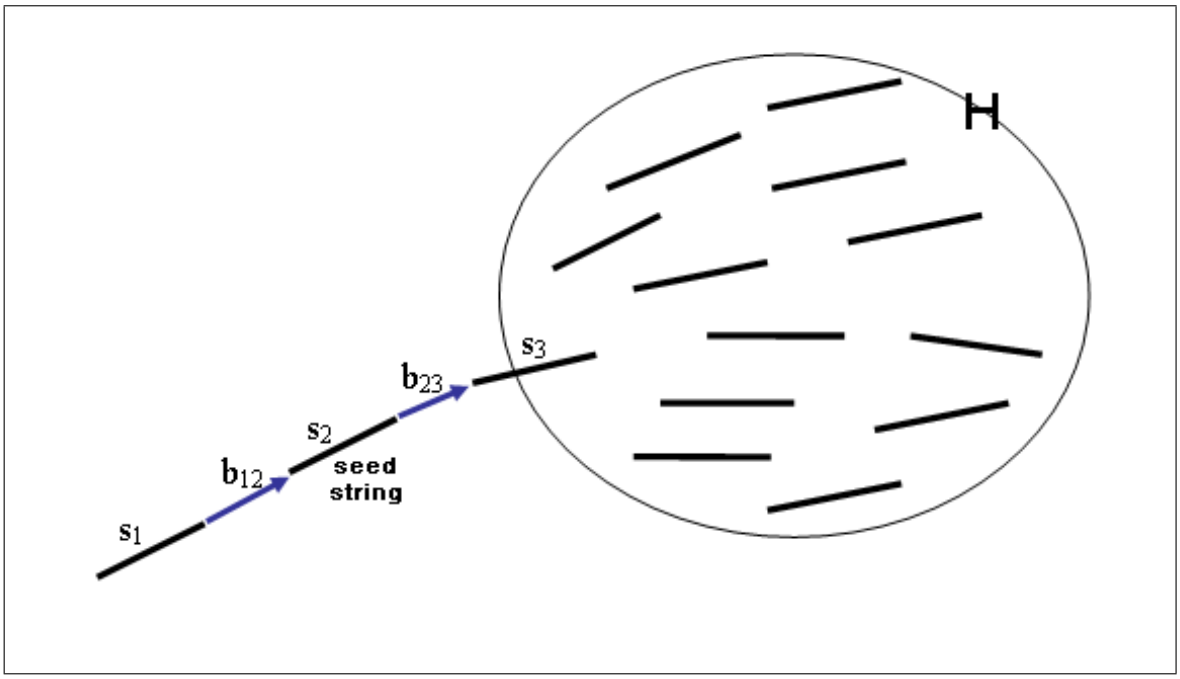

Figure 3.5. The grouped strings is cut at b_{34} selected randomly with a probability inversely proportional to its fitness value. H is the set of possible strings to make a new jump from the cut location

To obtain a new sample, a random jump is made at the broken jump location. This random jump is selected according to the probability of each possible jump that is calculated by Equation 3.2. After the new jump is found, we performed a new grouping as in Method 1 which is seen in Figure 3.6. Thus, the candidate generating density is

$$q(\underline{x},\underline{y}) = \left(\frac{\frac{1}{F_k}}{\sum_{w\in W}\frac{1}{F_w}}\right)\left(\frac{c(l)}{\sum_{h\in H}c(h)}\right) \tag{3.4}$$

where k is the selected jump to cut, W is all the possible jumps to cut, l is the newly selected jump and H is all the possible jumps that can be made at the location of the $k^{th} jump$.

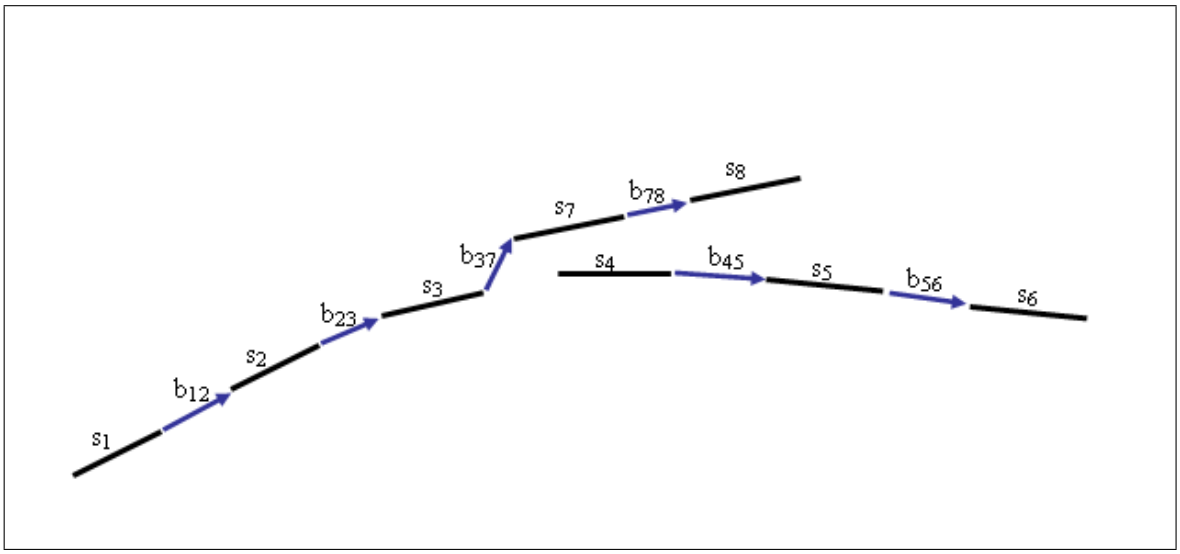

Figure 3.6. A random jump is made and a new grouping is done with this new jump.

This new group's fitness is set as the minimum jump fitness in this group and denoted by $f(\underline{y})$. The new group is accepted with a probability $\alpha(\underline{x}, \underline{y})$ as calculated in Equation 3.5 and if it is rejected the old group is counted once more.

For each combination of string pairs in the new accepted sample the corresponding elements of the co-occurrence matrix is increased by one. The same procedure is repeated for a seed string 300 times. This is done for the each string taken as a seed in the whole volume separately.

$$\alpha(\underline{x}, \underline{y}) = min\left(1, \frac{f(\underline{y})q(\underline{x}, \underline{y})}{f(\underline{x})q(\underline{y}, \underline{x})}\right) \tag{3.5}$$

The $q(\underline{y}, \underline{x})$ in the denominator in Equation 3.5 can be seen as having the candidate sample as current sample and calculating the probability of moving to the starting sample as shown in Figures 3.7 and 3.8. The probabilities $q(\underline{x}, \underline{y})$ and $q(\underline{y}, \underline{x})$ will

not be equal since the candidate selection region is different while constructing the candidate sample from initial one and the initial one from the candidate sample.

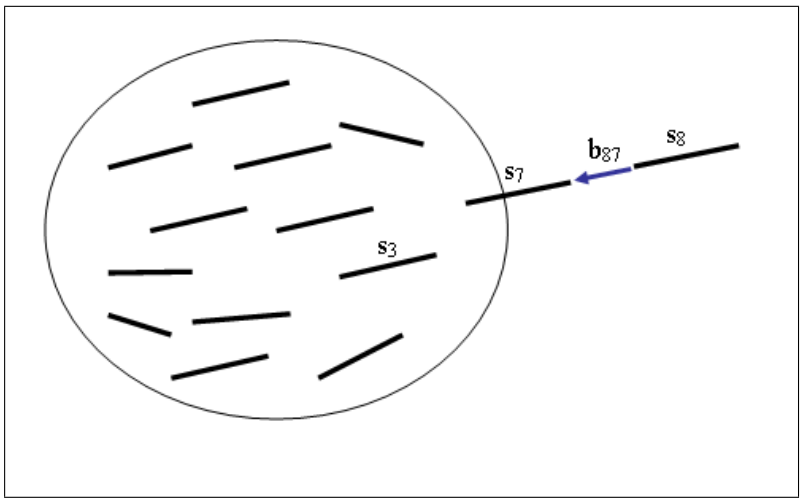

Figure 3.7. Candidate sample is cut from the newly constructed bridge.

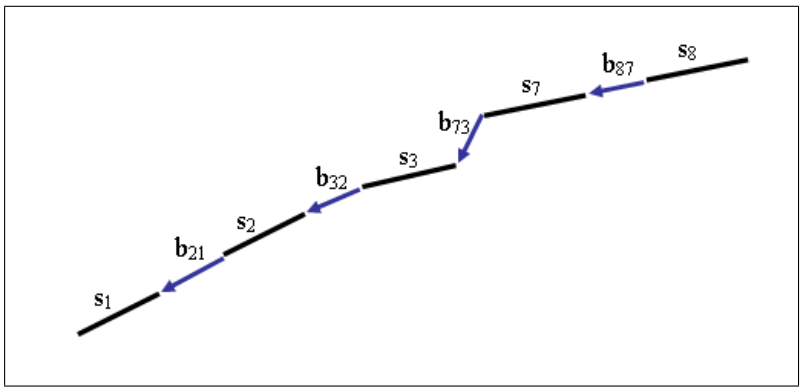

Figure 3.8. The starting sample is constructed from the cut candidate sample

4. EXPERIMENTS

4.1. Data

Whole brain DTI scanning was conducted on a 1.5T unit with 50mT/m maximum gradient strength using single-shot EPI scans. The scanning parameters were as follows:

- Field Of View(FOV)=24cm
- Matrix dimension = 128x128
- slice thickness/gap = 3.8mm/0mm
- Encoding directions = 12
- $b = 850 s/mm^2$
- gradient duration $\delta = 20ms$
- Frequency encoding = L/R

The total scanning time was around 3-4 minutes.

4.2. Direct Computation

The direct computation method for the creation of the co-occurrence matrix took around 25 seconds on an Intel Pentium IV machine with 2.4 GHz CPU speed and 1.5 GB ram. Total number of strings was 13540 in the whole volume. Calculated matrix is saved to hard disk to be utilized in visualization process. The resulting matrix had only 0.0014 percent non-zero elements. All the data used during fibertracking of short tracts and creation of co-occurrence matrix, is calculated and interpolated on the fly from the DTI tensor data. (i.e. extraction of eigenvectors, eigenvalues and FA values). The visualization of fiber tracts passing through a selected region is shown on Figure 4.1. The figure shows the Pyramidal Tracks.

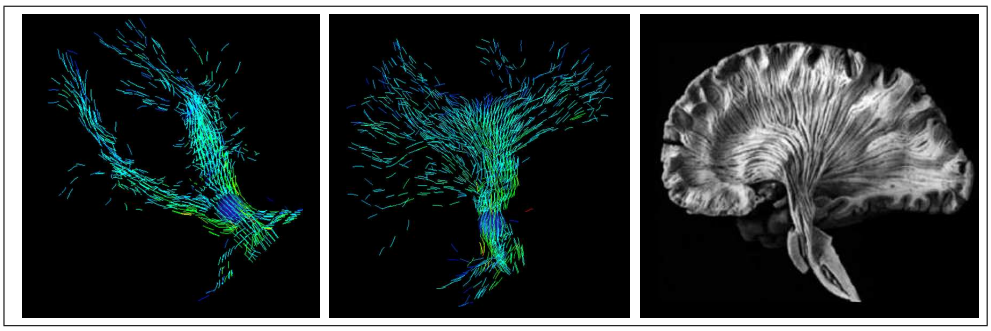

Figure 4.1. Visualization of strings that pass from a selected region at pyramidal tracts using Direct Computation Method viewing from different angles. The right most figure shows the anatomical image.

4.3. Metropolis-Hastings

The Metropolis-Hastings method took around 170 minutes to create the co-occurrence matrix. Again the total number of strings was 13540 in the whole volume. After 150 iterations the co-occurrence matrix has 0.0037 percent non-zero elements and after 300 iterations 0.0663 elements was non-zero. Figure 4.2 shows the visualization of fibertracts which passes through the same selected point as shown in Figure 4.1

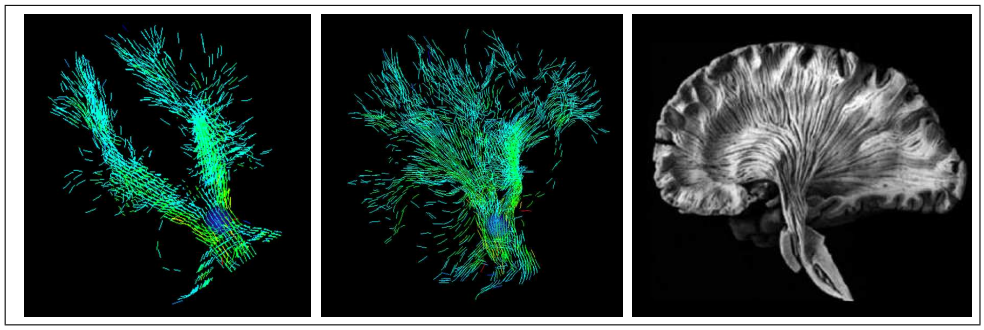

Figure 4.2. Visualization of strings that pass from a selected region at pyramidal tracts using Metropolis Hastings Method viewing from different angles. The right most figure shows the anatomical image.

5. DISCUSSION

The most important disadvantage of MR-DTI is that there is no gold standards defined in this area of study.Hence the results are compared with the anatomical results that are obtained from previous works.

One of the advantages of proposed SMT method is the multipath consideration of fibertracts.

Also SMT with Metropolis-Hastings method takes account the stochastic nature of the underlying data. Since diffusion is a random process with a probability distribution the results obtained from this data should have a corresponding probability values. Metropolis-Hastings method labels fibertract distributions according to their uncertainty.

Another advantage of SMT that it allows branching of fiber paths. Thus each seed location is allowed to end up more than one location. This is an important issue especially at locations where a lot of fiber paths come closer and seem to merge. At these locations only one fiber path is obtained when tracking is started at the merged location with conventional fiber tracking methods.

When considering the visualization of fiber tracts, SMT provides a true visualization of results. It does not hide any possible tracts. Users can interactively hide less probable tracts with the provided interaction tools.

5.1. Comparison of fibertracking results at Corpus Callosum

On figure 5.1 the left image shows the anatomical structure of the corpus callosum which is the structure deep in the brain that connects the right and left hemispheres of the cerebrum, coordinating the functions of the two halves. We applied both continues fiber tracking and split and merge methods from a selected are in this region. The

middle image shows both the continues tract and the probability distribution obtained from Metropolis-Hastings method. In right image we applied a threshold value to visualize the more probable tracts. It is seen that the expected tract of the distribution is similar to the continues tract.

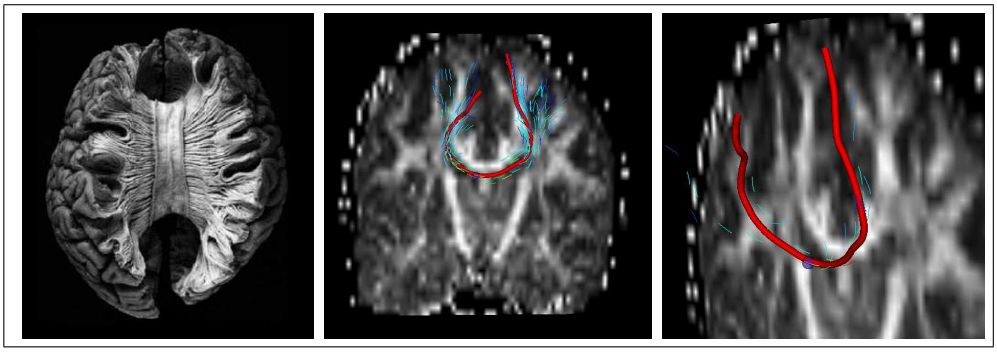

Figure 5.1. Comparison of fibertracting result at corpus callosum Left: Anatomic image[36] Middle:Metropolis-Hastings Method Right: A threshold is applied to Metropolis-Hastings method

5.2. Comparison of fibertracking results at Pyramidal Tracts

On figure 5.2 pyramidal tracts are shown in the left anatomical image. These tracts controls the distal limbs such as the fingers, hands, toes which can require fine motor control. The middle image again shows the results obtained from both continues 4^{th} order Runge-Kutta and Metropolis-Hastings method. Less probable paths are filtered by setting a threshold value to the co-occurrence matrix on the right image. Both result obtained by different techniques are similar to each other.

More comparison figures of Direct Computation and Metropolis-Hastings Method can be seen in Appendix C.

Of course these visualized tracts always should be taken as probability distributions and can be filtered by the GUI interactively to see the most co-occurred string pairs.

It is shown that due to the limitations of fibertractography approaches and DTI

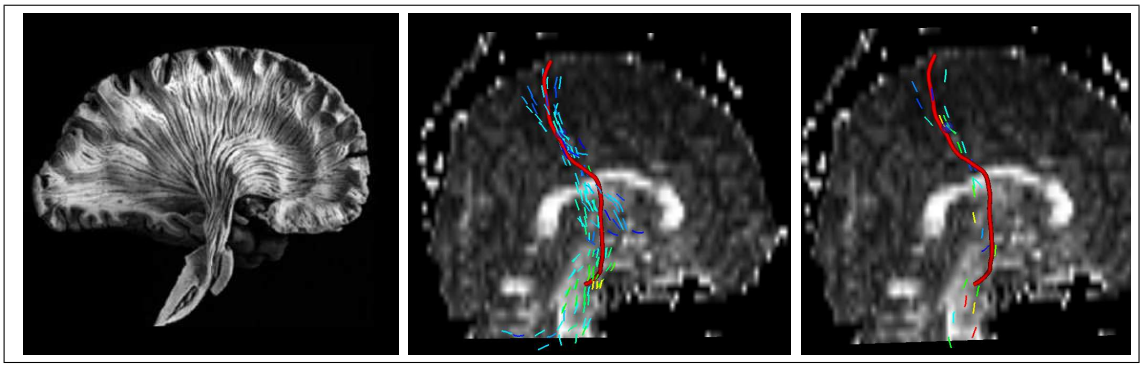

Figure 5.2. Comparison of methods at pyramidal tracts . Left: Anatomic image[36] Middle:Metropolis-Hastings Method Right: A threshold is applied to Metropolis-Hastings method

data, it is is not possible to obtain one true fiber path for a seed point in the brain. This is mainly due to the low resolution of DTI data which does not have the enough resolution to solve the partial volume effects. The data has only the averaged values of microscopic scaled anatomical structures in a macroscopic scale.

5.3. Comparison of experiment results

In the experiments we compared two different quantities derived from Direct Computation and Metropolis-Hastings method. One of the quantities is the number of different connections that is made by a seed string. The result is shown on figure 5.3.

The figure 5.3 is colored by the number of different string connections with the string that is seeded from the pixel. The number of connections is increased by the iteration number compared to Direct Computation and low iteration values. While the direct computation method results in an average of 30 different connections from a seed string, this number highly increases in Metropolis-Hastings Method. This should be interpreted such that as the number of iterations is increased the obtained tract paths are the possible samples from the underlying tract probability distribution.

An other quantity derived from the experiments is the length of the maximum path obtained by both methods. Each pixel color represents the maximum length of the

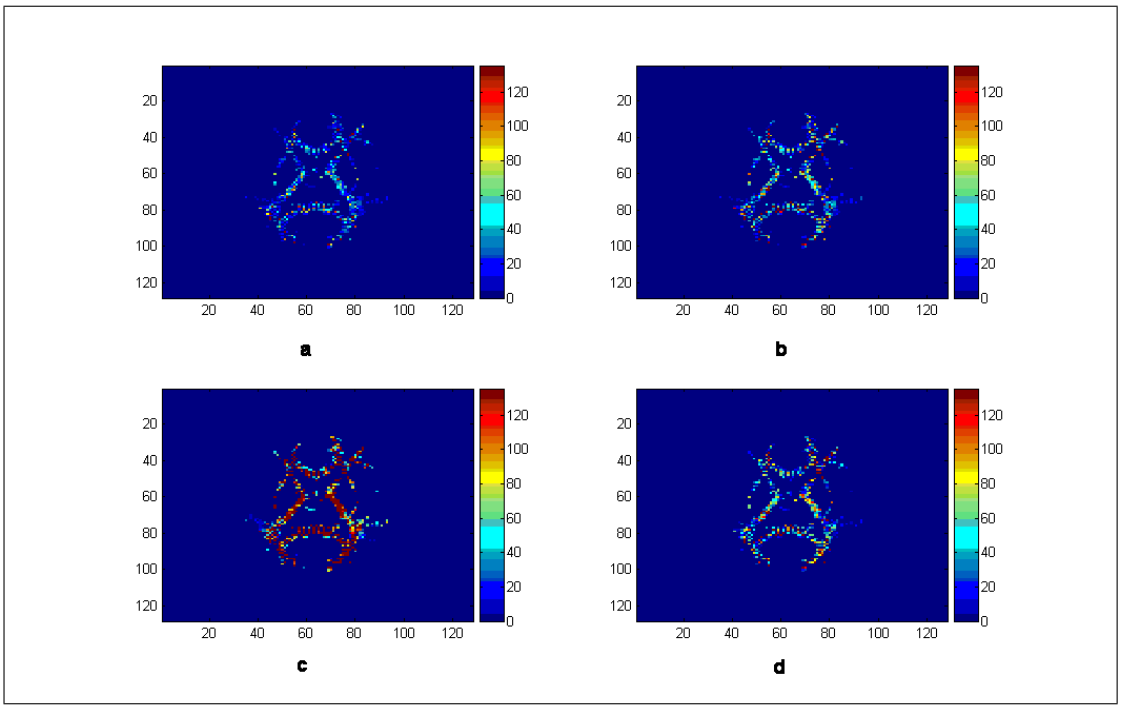

Figure 5.3. The color represents the number of different connections with other strings from the pixel a)Direct computation result. b)Result after 150 iterations c)Result after 300 iterations d)Difference between direct computation and 300 iteration metropolis-hastings method

grouped strings. Again it is obvious in figure 5.4 that maximum length of the possible tracts are increased for most of the seed strings as compared to the maximum distance obtained from Direct Computation method and low iteration values of Metropolis-Hastings algorithm.

In general there are some parametric issues in general about the Metropolis-Hastings algorithms which is a Monte Carlo Markov Chain method. These problems can be stated as;

- The number of iterations
- Using an efficient transition function to generate new candidates
- Number of iterations to be omitted for preventing the starting bias introduced by starting sample

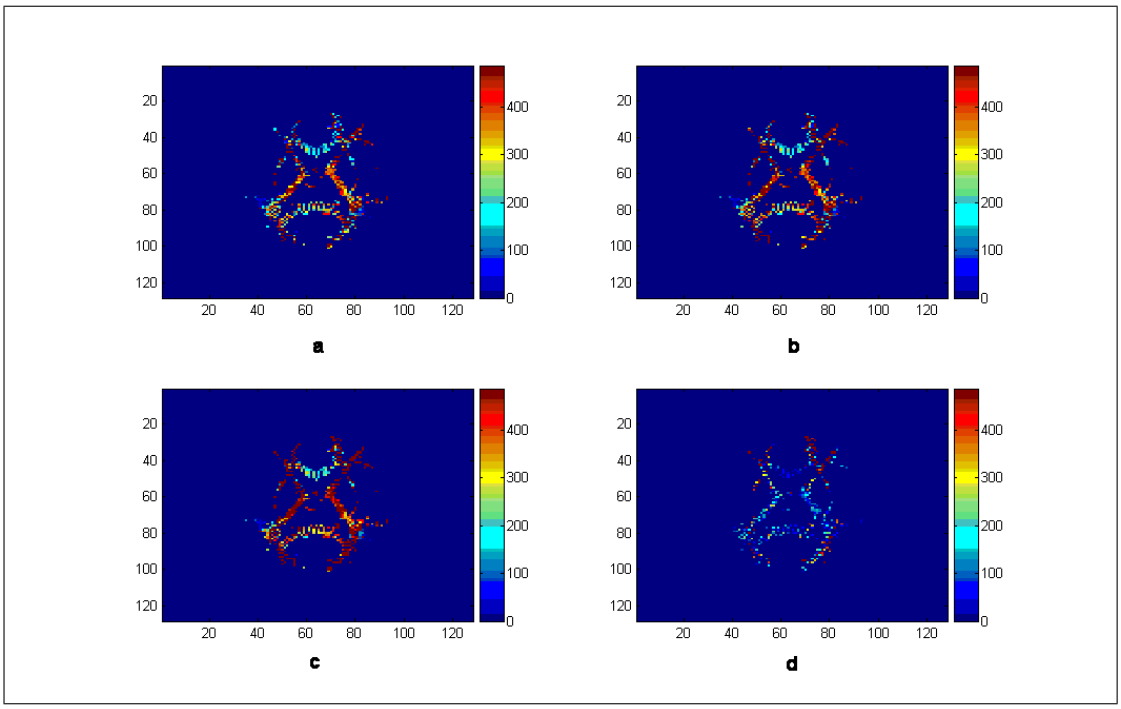

Figure 5.4. The color represents the maximum distance of a connection from that pixel in millimeters a)Direct computation result. b)Result after 150 iterations c)Result after 300 iterations d)Difference between direct computation and 300 iteration metropolis-hastings method

Other than the issues regarding the Metropolis-Hastings algorithm there are also problems about the parameters of the visualization system. One of them is the selection of the correct value for the threshold of the co-occurrence matrix. Since there are no gold standards about the Diffusion Tensor Imaging these parameters are highly dependent to the experience of the users.

6. IMPLEMENTATION

6.1. Graphical User Interface

Fast Light Toolkit (FLTK), which is a cross-platform, free software, GUI library is used for graphical user interface (GUI) implementation. It is written in C++ and is functional on Windows, GNU/Linux, Mac OS X, Solaris, OS/2, and other Unix and Unix-like operating systems.

FLTK provides GUI functionality without bloat and supports 3D graphics via OpenGL and its built-in GLUT emulation. FLTK is designed to be small and modular enough to be statically linked. FLTK can also be used as a shared library, which is now being included on some Linux distributions [31].

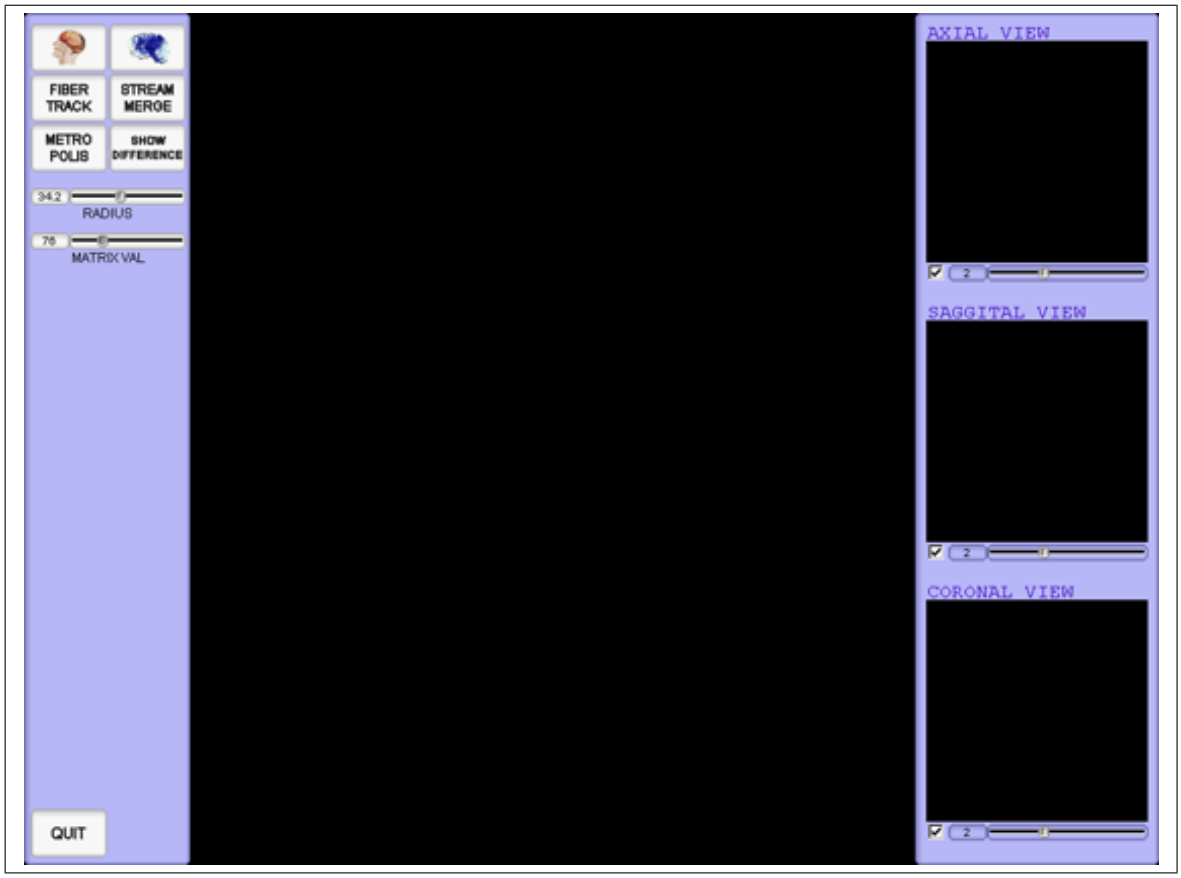

Figure 6.1. Screenshot of user interface.

6.2. Visualization

Visualization Toolkit (VTK) which is an open source, freely available software system for 3D computer graphics, image processing, and visualization is used for the visualization tasks. VTK consists of a C++ class library, and several interpreted interface layers including Tcl/Tk, Java, and Python. VTK supports a wide variety of visualization algorithms including scalar, vector, tensor, texture, and volumetric methods; and advanced modeling techniques such as implicit modeling, polygon reduction, mesh smoothing, cutting, contouring, and Delaunay triangulation. In addition, dozens of imaging algorithms have been directly integrated to allow the user to mix 2D imaging / 3D graphics algorithms and data. VTK is a powerful platform independent graphics engine with parallel rendering support [30].

6.3. Image Processing

All the image processing and algorithms is developed in C++. VXL (the Vision-something-Libraries) which is a collection of C++ libraries designed for computer vision research and implementation is also used for matrix operations. VXL is written in ANSI/ISO C++ and is designed to be portable over many platforms. VXL provides easy implementation of algorithms with high performance arithmetic operations and matrix algorithms [29].

7. CONCLUSION

This thesis introduced a new technique for the visualization of fiber tracts. The proposed Split/Merge Method tries to overcome the disadvantages of existing visualization techniques. It considers that voxels are likely to consist of contributions from multiple tissues and there may not be a single predominant direction of water diffusion, also related to the macroscopic character of DTI the mixing of axonal tracts with different orientations within a voxel is taken into account. To overcome those problems this technique allows branching of fibertracts and local data structure in the volume can be easily estimated by the visualized orientation of strings at that point. This allows users to have an idea of the local coherency in the fiber tracts and can interactively select regions they are interested in to study in detail.

Split/Merge method does not assumes any fiber paths for 100 percent sure, instead it visualizes a distribution of paths with different probabilities which can be filtered interactively to see the possible paths. Since diffusion can be regarded as a probability distribution of particles in a defined volume , the diffusion in the brain should result also in a probability distribution of different paths. The Metropolis-Hastings method suggested in this thesis tries to converge to the underlying probability of the fiber tracts in the brain and to overcome the current limitations of fiber tractography.

Also the usage of Log-Euclidean Framework for the interpolation of tensors provides the conservation of anisotropy in interpolated tensors.

For the future studies different methods can be implemented for the creation of co-occurrence matrix which can increase the performance and can converge better to the real probability distribution of the underlying data. Also different transition functions can be implemented for a better performance of Metropolis-Hastings Method.

APPENDIX A: Log-Euclidean Framework

Tensors, i.e. symmetric positive-definite matrices in medical imaging, appear in many contexts: Diffusion Tensor MRI, modeling of anatomical variability, etc. They are also a general tool in image analysis, especially for segmentation, motion and texture analysis. In order to carry out general computations on these objects, one needs a consistent operational framework. This is necessary to completely generalize to tensors statistical tools and Partial Differential Equations (PDEs). The framework of Riemannian metrics has recently emerged as particularly adapted to this task [24].

One can directly use a Euclidean structure on square matrices to define a metric on the tensor space, for instance with the following distance: $dist^2(S_1, S_2) = (Trace((S_1 - S_1)^2))$. This is straightforward and leads a priori to simple computations. But this framework is practically and theoretically unsatisfactory for three main reasons. First, symmetric matrices with null or negative eigenvalues appear during Euclidean computations. And from a physical point of view, in DTI, a diffusion exactly equal to zero is impossible: above 0 Kelvin, water molecules will move in all directions. Even worse, a negative diffusion is meaningless. This occurs during iterated Euclidean computations, for instance during the estimation of tensors from diffusion-weighted images, the regularization of tensors fields, etc. To avoid going out of the tensor space, it has been proposed to regularize only features extracted from tensors, like first eigenvectors [26] or orientations [25]. The regularization is propagated to tensors in a second step. This is not completely satisfactory, since it would be preferable to regularize tensors directly in order to take into account all the information they carry.

Second, a tensor corresponds typically to a covariance matrix. The value of its determinant is a direct measure of the dispersion of the associated multivariate Gaussian. The reason is that the volume of associated confidence regions are proportional to the square root of the covariance determinant. But the Euclidean averaging of tensors leads very often to a tensor swelling effect: the determinant (and thus the dispersion) of the Euclidean mean can be larger than the original determinants! In DTI, diffusion

tensors are assumed to be covariance matrices of the local Brownian motion of water molecules. Introducing more dispersion in computations amounts to introducing more diffusion, which is physically unacceptable.

Third, the Euclidean metric is unsatisfactory in terms of symmetry with respect to matrix inversion. The Euclidean mean for tensors is an arithmetic mean which does not yield the identity for a tensor and its matrix inverse. When tensors model variability, one would rather have in many cases a geometric mean.

To fully circumvent these difficulties, affine-invariant Riemannian metrics have been recently proposed for tensors in [27]. With them, negative and null eigenvalues are at an infinite distance, the swelling effect disappears and the symmetry with respect to inversion is respected. The price paid for this success is a high computational burden, essentially due to the curvature induced on the tensor space. Practically, this yields slow and hard to implement algorithms.

A new Riemannian framework to fully overcome these computational limitations while preserving excellent theoretical properties is proposed by Log-Euclidean framework. It is based on new metrics named Log-Euclidean, which are particularly simple to use. They result in classical Euclidean computations in the domain of matrix logarithms.

A.1. Existence and Uniqueness of the Logarithm

A tensor S has a unique symmetric matrix logarithm L = log(S). It verifies S = exp(L) where exp is the matrix exponential. Conversely, each symmetric matrix is associated to a tensor by the exponential. L is obtained from S by changing its eigenvalues into their natural logarithms, which can be done easily in an orthonormal basis in which S (and L) is diagonal.

A.2. Euclidean Calculus in the Logarithmic Domain

The tensor vector space with a Log-Euclidean metric is in fact isomorphic (the algebraic structure of vector space is conserved) and isometric (distances are conserved) with the corresponding Euclidean space of symmetric matrices. As a consequence, the Riemannian framework for statistics and analysis is extremely simplified [28]. In particular, the Log-Euclidean mean of N tensors with arbitrary positive weights $(w^i)_{i=1}^N$ such that $\sum_{i=1}^N w^i = 1$ is a direct generalization of the geometric mean of positive numbers and is given explicitly by:

$$E_{LE}(S_1, ..., S_N) = exp(\sum_{i=1}^{N} w^i log(S_i)) \tag{A.1}$$

This is remarkable: in this framework, the processing of tensors is simply Euclidean in the logarithmic domain. Final results obtained on logarithms are mapped back to the tensor domain with the exponential. Hence, statistical tools or PDEs are readily generalized to tensors in this framework.

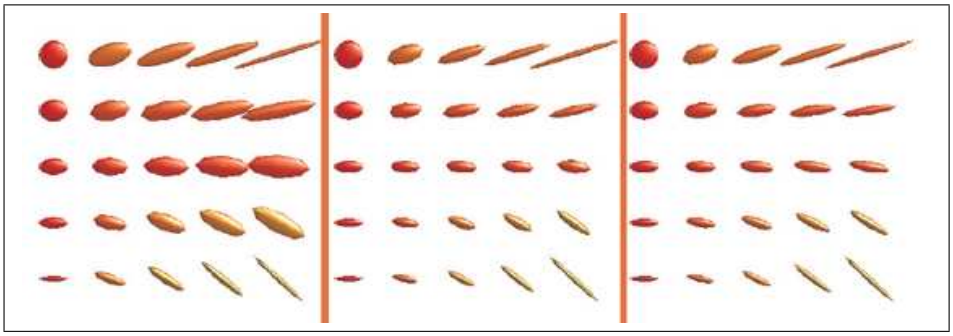

Figure A.1. Bilinear interpolation of 4 tensors at the corners of a grid. Left: Euclidean interpolation. Middle: affine-invariant interpolation. Right: Log-Euclidean interpolation. Log-Euclidean means are slightly more anisotropic than their affine-invariant counterparts. The coloring of ellipsoids is based on the direction of dominant eigenvectors. [27]

APPENDIX B: Metropolis-Hastings Algorithm

This powerful algorithm provides a general approach for producing a correlated sequence of draws from the target density that may be difficult to sample by a classical independence method. The goal is to simulate the d-dimensional distribution $\pi^*(\psi)$, $psi \in \Psi \subseteq \Re^d$ that has density $\pi(\psi)$ with respect to some dominating measure. To define the algorithm, let $q(\psi, \psi')$ denote a source density for a candidate draw ψ' given the current value ψ in the sampled sequence. The density $q(\psi, \psi')$ is referred to as the proposal or candidate generating density. Then, the M-H algorithm is defined by two steps: a first step in which a proposal value is drawn from the candidate generating density and a second step in which the proposal value is accepted as the next iterate in the Markov chain according to the probability $\alpha(\psi, \psi')$ $\alpha(\psi, \psi')$, where

$$\alpha(\psi, \psi') = min\left[\frac{\pi(\psi')q(\psi', \psi)}{\pi(\psi)q(\psi, \psi')}, 1\right] \qquad \textbf{if} \qquad \pi(\psi)q(\psi, \psi') > 0 \tag{B.1}$$

$$\alpha(\psi, \psi') = 1 \quad \textbf{otherwise} \tag{B.2}$$

If the proposal value is rejected, then the next sampled value is taken to be the current value.

Typically, a certain number of values at the start of this sequence are discarded after which the chain is assumed to have converged to it invariant distribution and the subsequent draws are taken as approximate variates from π. Because theoretical calculation of the burn-in is not easy it is important that the proposal density is chosen to ensure that the chain makes large moves through the support of the invariant distribution without staying at one place for many iterations. Generally, the empirical behavior of the M-H output is monitored by the autocorrelation time of each component of ψ and by the acceptance rate, which is the proportion of times a move is made as the sampling proceeds [35].

One should observe that the target density appears as a ratio in the probability $\alpha(\psi, \psi')$ and therefore the algorithm can be implemented without knowledge of the normalizing constant of $\pi(\cdot)$. Furthermore, if the candidate-generating density is symmetric, i.e. $q(\psi', \psi) = q(\psi, \psi')$, the acceptance probability only contains the ratio $\pi(\psi')/\pi(\psi)$ hence, if $\pi(\psi') > \pi(\psi)$ the chain moves to ψ' otherwise it moves with probability given by $\pi(\psi')/\pi(\psi)$

APPENDIX C: Comparison Figures of Direct Computation Method and Metropolis-Hastings Results

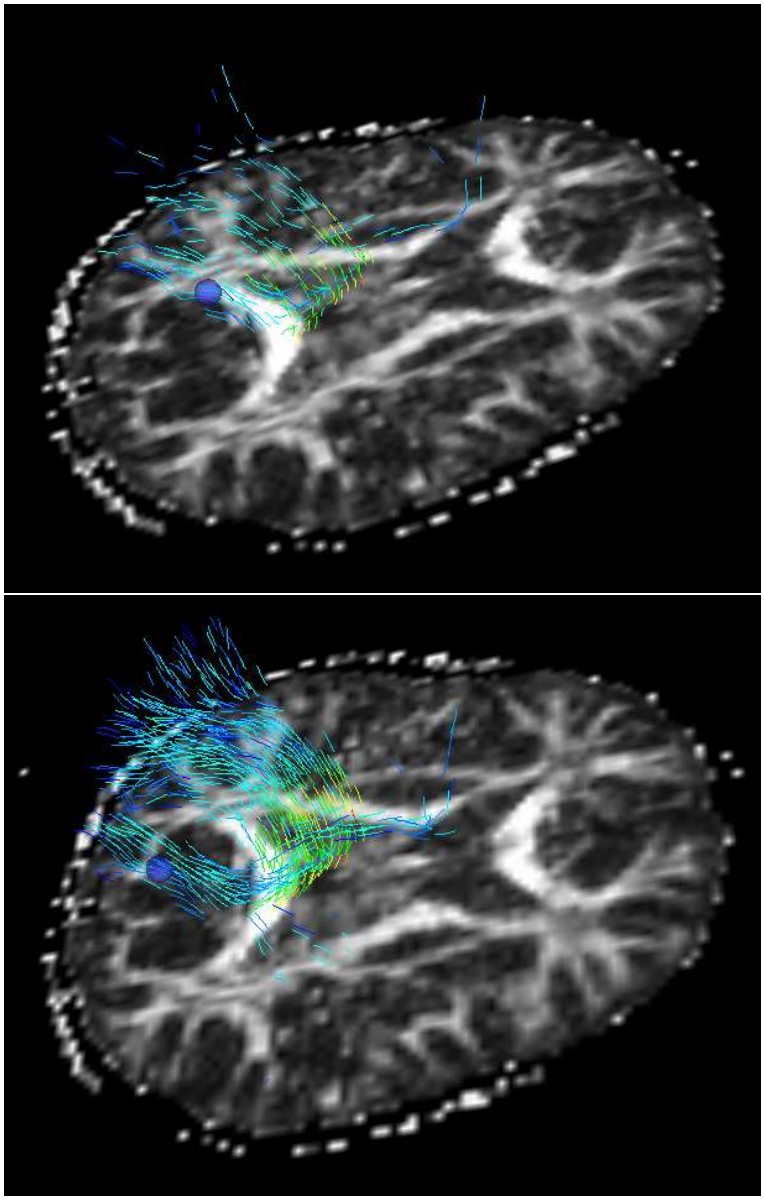

Figure C.1. Snapshots from the results of grouping with different methods. **Up**: Direct Computation Method **Down**: Metropolis-Hastings Method

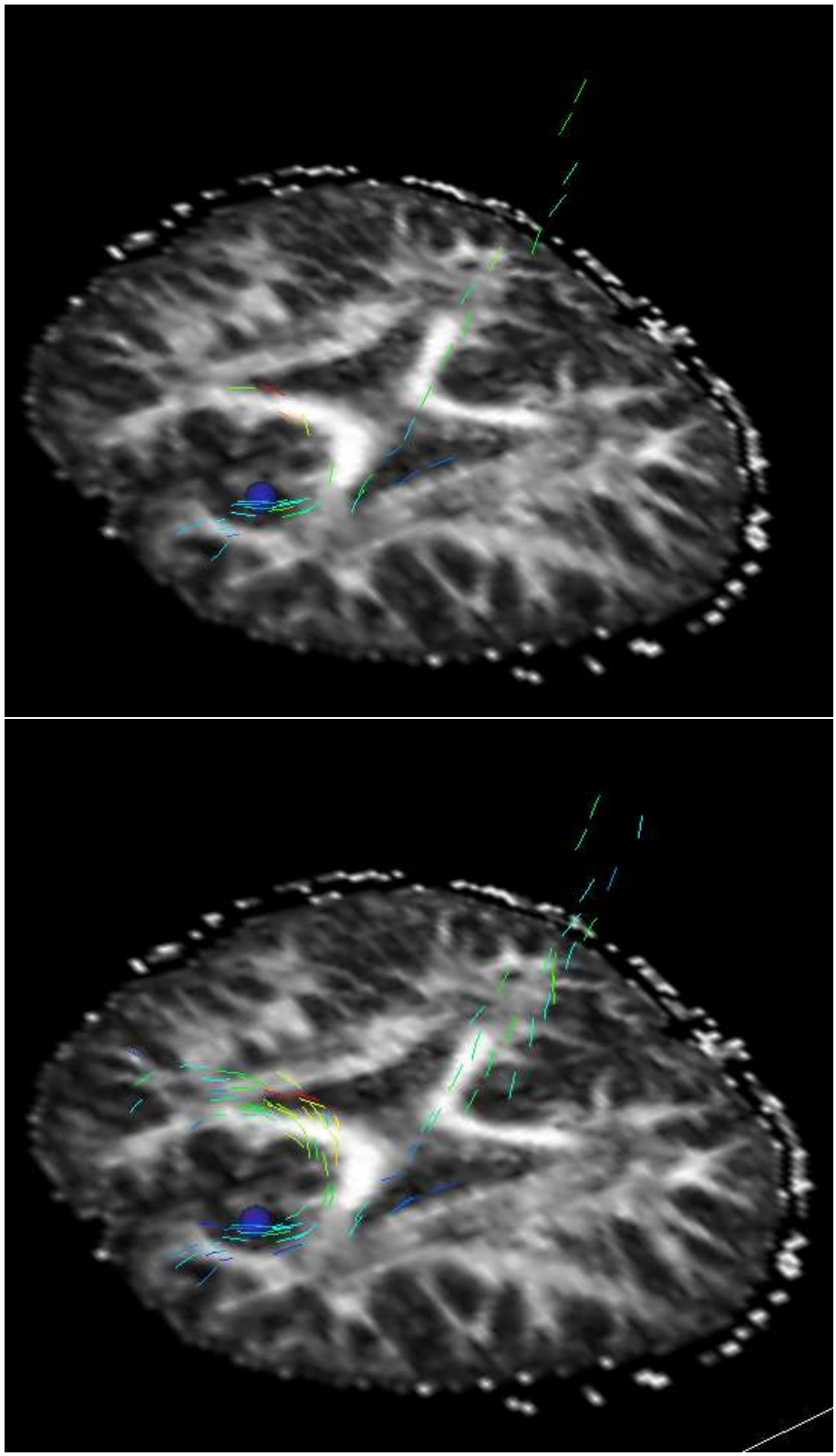

Figure C.2. Snapshots from the results of grouping with different methods. **Up**: Direct Computation Method **Down**: Metropolis-Hastings Method

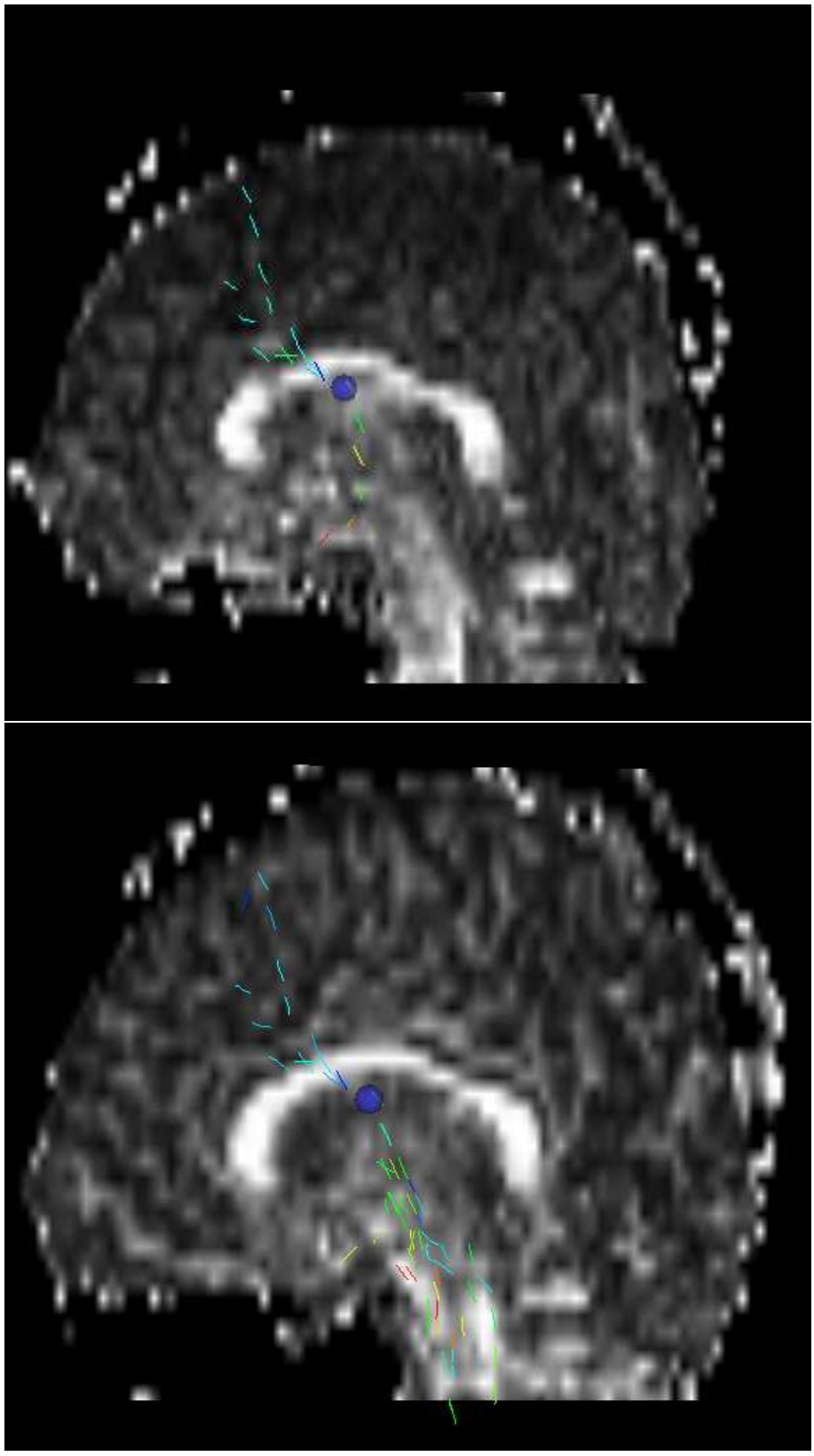

Figure C.3. Snapshots from the results of grouping with different methods.
Up: Direct Computation Method **Down**: Metropolis-Hastings Method

REFERENCES

1. David S. Tuch,Timothy G. Reese,Mette R. Wiegell,Nikos Makris, John W. Belliveau, and Van J.Wedeen, "High Angular Resolution Diffusion Imaging Reveals Intravoxel White Matter Fiber Heterogeneity", *Magnetic Resonance in Medicine*, Vol. 48, pp. 577-582, 2002.

2. David Solomon Tuch, "Diffusion MRI of Complex Tissue Structure", *Ph.D. thesis*, Massachusetts Institute of Technology, 2002.

3. Alexander J. Taylor, "Diffusion Tensor Imaging: Evaluation of Tractography Algorithm Performance Using Ground Truth Phantoms", *MSc. Thesis*, Virginia Polytechnic Institute and State University, May 2004.

4. Richard Watts, Conor Liston, Sumit Niogi and Aziz M. Uluğ, "Fiber Tracking using Magnetic Resonance Diffusion Tensor Imaging and its Applications to Human Brain Development", *Departments of Radiology, Psychiatry and Neuroscience*, Weill Medical College of Cornell University.

5. Peter J. Basser, James Mattiello, and Denis Lebihan, "Estimation of the Effective Self-Diffusion Tensor from the NMR Spin Echo", *Journal of Magnetic Resonance*, Series B 103, pp. 247–254, 1992.

6. Peter J. Basser, James Mattiello, and Denis Lebihan, "MR Diffusion Tensor Spectroscopy and Imaging", *Biophysical Journal*, Vol. 66, pp. 259–267, 1994.

7. Peter J. Basser, Sinisa Pajevic, Carlo Pierpaoli, Jeffrey Duda, and Akram Aldroubi, "In Vivo Fiber Tractography Using DT-MRI Data", *Magnetic Resonance in Medicine*, Vol. 44, pp. 625–632, 2000.

8. Peter J. Basser, and Derek K. Jones, "Diffusion-tensor MRI: theory, experimental design and data analysis – a technical review", *NMR in Biomedicine*, Vol. 15,

pp.456–467, 2002.

9. Mats Björnemo, Anders Brun, "White Matter Fiber Tracking Using Diffusion Tensor MRI", *MSc. Thesis*, Linköping University, Biomedical Engineering Department, 28 February 2002.

10. Howard C. Berg, "Random Walks in Biology", *Princeton University Press* , Princeton, NJ, 1983.

11. Mariana Lazar, "White Matter Tractography: An Error Analysis and Human Brain Fiber Tract Reconstruction Study", *Ph.D. thesis*, The University of Utah ,Department of Physics May 2003.

12. C.R. Tench, P.S. Morgan, M. Wilson, and L.D. Blumhardt, "White Matter Mapping Using Diffusion Tensor MRI", *Magnetic Resonance in Medicine*, Vol. 47, pp. 967–972, 2002.

13. Geoffrey J. M. Parker, Claudia A. M. Wheeler-Kingshott, and Gareth J. Barker, "Estimating Distributed Anatomical Connectivity Using Fast Marching Methods and Diffusion Tensor Imaging", *IEEE TRANSACTIONS ON MEDICAL IMAGING*, Vol. 21, No.5, May 2002.

14. Jennifer S. W. Campbell, Kaleem Siddiqi, Baba C. Vemuri and G. Bruce Pike, "A GEOMETRIC FLOWFOR WHITE MATTER FIBRE TRACT RECONSTRUCTION", *McGill University*, University of Florida, IEEE 0-7803-7584-X/02, 2002.

15. P. Hagmann,J.-P. Thiran, L. Jonasson, P. Vandergheynst, S. Clarke, P. Maeder, and R. Meulib, "DTI mapping of human brain connectivity: statistical fibre tracking and virtual dissection", *NeuroImage*, Vol. 19, pp. 545–554, 2003 .

16. Erdem Yörük, Burak Acar, and Roland Bammer, "A Physical Model for DT-MRI Based Connectivity Map Computation", *Lecture Notes in Computer Science*, Vol. 3749 / Part 1, pp. 213–220, Springer, 2005.

17. S. Jbabdi, P. Bellec, G. Marrelec, V. Perlbarg, H. Benali, "A Level Set Method For Building Anatomical Connectivity Paths Between Brain Areas Using DTI", *INSERM U494*, Paris, France, 2004.

18. C.R. Tench, P.S. Morgan, L.D. Blumhardt, and C. Constantinescu, "Improved White Matter Fiber Tracking Using Stochastic Labeling", *Magnetic Resonance in Medicine*, Vol. 48 pp. 677-683, 2002.

19. David S. Tuch, Timothy G. Reese, Mette R. Wiegell, Nikos Makris, John W. Belliveau, and Van J. Wedeen, "High Angular Resolution Diffusion Imaging Reveals Intravoxel White Matter Fiber Heterogeneity", *Magnetic Resonance in Medicine*, Vol. 48 pp. 577-582, 2002.

20. Roland Bammer, Burak Acar, Michael E. Moseley, "In vivo MR tractography using diffusion imaging", *European Journal of Radiology*, Vol. 45 pp. 223-234, 2003.

21. Ning Kang, Jun Zhang, Eric S. Carlson, and Daniel Gembris, "White Matter Fiber Tractography Via Anisotropic Diffusion Simulation in the Human Brain", *IEEE Transactions on Medical Imaging*, Vol. 24, No. 9, September 2005.

22. Vincent Arsigny, Pierre Fillard, Xavier Pennec, and Nicholas Ayache, "Fast and Simple Calculus on Tensors in the Log-Euclidean Framework", *INRIA Sophia - Projet Epidaure*,Sophia Antipolis Cedex, France.

23. Siddhartha Chib Edward Greenberg, "Understanding the Metropolis Hastings Algorithm", *The American Statistician*, Vol. 49, pp.327, No 1995.

24. Xavier Pennec, "Probabilities and statistics on Riemannian manifolds: a geometric approach", *Research Report 5093*, INRIA, January 2004.

25. C. Chefdhotel, D. Tschumperle, R. Deriche, and O. Faugeras, "Regularizing flows for constrained matrix-valued images", *J. Math. Im. Vis.*, Vol. 20, pp. 147-162, 2004.

26. O. Coulon, D. Alexander, and S. Arridge, "Diffusion tensor magnetic resonance image regularization", *Medical Image Analysis*, Vol. 8, pp. 4767, 2004.

27. Xavier Pennec, Pierre Fillard, and Nicholas Ayache, "A Riemannian framework for tensor computing", *Research Report 5255*, INRIA, July 2004.

28. V. Arsigny, P. Fillard, X. Pennec, and N. Ayache, "Fast and simple computations on tensors with Log-Euclidean metrics", *Research Report 5584*, INRIA, May 2005.

29. http://vxl.sourceforge.net

30. http://en.wikipedia.org/wiki/VTK

31. http://en.wikipedia.org/wiki/FLTK

32. Stephanie Y. Lee, Stephen Correia, David F. Tate, Robert H. Paul3, Song Zhang, Stephen P. Salloway, Paul F. Malloy, and David H. Laidlaw, "Quantitative Tractography Metrics for White Matter Integrity Based on Diffusion Tensor MRI Data"

33. Song Zhang, Demiralp, C., and Laidlaw, D., "Visualizing diffusion tensor MR images using streamtubes and streamsurfaces", *IEEE Transactions on Visualization and Computer Graphics*, Vol. 9 , pp.454–462.

34. Olivier Coulon, "Imagerie mdicale, imagerie crbrale, imagerie par rsonance magntique", http://www.esil.univ-mrs.fr

35. http://www.quantlet.com/mdstat/scripts/csa/html/node27.html

36. http://www.vh.org/Providers/Textbooks/BrainAnatomy/TOC.html